# Benchmarking three-dimensional metal foam electrodes for the electrochemical reduction of nitrate

Yenny Maribel Allcca Castillo, Yanis Adjez, Victor Raul Jauja Ccana, Gabriel Cerrón-Calle, Sergi Garcia-Segura, Adolfo La Rosa-Toro Gómez, Carlos M Sánchez-Sánchez

▶ **To cite this version:**

# Benchmarking Three-Dimensional Metal Foam Electrodes for the Electrochemical Reduction of Nitrate

Yenny Maribel Allcca Castillo[a], Yanis Adjez[b], Victor Raul Jauja Ccana[a], Gabriel A. Cerrón-Calle[c], Sergi Garcia-Segura[c], Adolfo La Rosa-Toro Gómez[a]*, Carlos M. Sánchez-Sánchez[b]**

[a]Laboratorio de Investigación de Electroquímica Aplicada, Facultad de Ciencias, Universidad Nacional de Ingeniería, Av. Túpac Amaru 210, Rimac, Lima, Perú.

[b]Sorbonne Université, CNRS, Laboratoire Interfaces et Systèmes Electrochimiques, LISE, 4 Place Jussieu, 75005, Paris, France.

[c]Nanosystems Engineering Research Center for Nanotechnology-Enabled Water Treatment, School of Sustainable Engineering and the Built Environment, Arizona State University, Tempe, AZ 85287-3005, USA

Review article to be published in Journal of Electroanalytical Chemistry

Corresponding authors:

* toro@uni.edu.pe

** carlos.sanchez@sorbonne-universite.fr

**Abstract**

The electrochemical reduction of nitrate (ERN) is a promising and sustainable strategy for addressing the critical issue of nitrate pollution in water sources. The rational design of electrocatalysts has spotlighted metal-based three-dimensional (3D) electrodes such as Cu and Ni foams. Metallic Cu foam showcases promising kinetics for ERN conversion, while Ni foam serves as a robust support material for self-standing catalyst evaluation. This review underscores the nuances and challenges in ERN research when exploiting 3D electrodes, emphasizing the overlooked roles of pore per inch (*PPI*) and electrochemically active surface area (ECSA), as well as the lack of standardization and inconsistent reporting practices, which hinders direct performance comparison among different ERN studies. The *PPI* value controls reactant and products mass transfer at the interface and impacts on the magnitude and extension of the solution alkalinization at the electrode surface, while ECSA is essential for accurately comparing the specific electrocatalytic activity of metal foam electrodes for ERN. Particular attention is devoted to modified self-standing 3D electrode materials, where the catalytic performance on either Cu or Ni foams is altered by adding other metals and/or metal oxides ($Cu_{foam}$/M) and ($Ni_{foam}$/M), respectively. A detailed analysis of selected modified Cu and Ni foam electrocatalysts available in the literature is provided to demonstrate the lack of standardization reporting ERN performance at present. Thus, we propose the adoption of more rigorous characterization and reporting practices to advance the development of efficient and scalable ERN systems for sustainable water treatment. This includes *PPI* value, ECSA determination and additional engineering figures of merit encompassing both selectivity and conversion such as $NH_3$ generation efficiency (%) and ERN energy efficiency (%). Parameters such as nitrate conversion, faradaic efficiency and selectivity, often used as benchmarks, are considered not suitable enough for comparing different ERN studies because they depend on the initial nitrate concentration, the total charge circulated and the type of electrolysis (galvanostatic or potentiostatic).

**Keywords**: Nitrate reduction; Electrocatalysis; Cu foam; Ni foam; Benchmark; ECSA

## 1. Introduction

The never-ending search for water treatment alternatives to secure access to potable water has advanced our understanding of technologies in the water-energy nexus [1,2]. Electrocatalysis has been positioned as one of the most promising emerging sustainable technologies, transforming pollutants into harmless compounds or added-value products without introducing extra chemicals [3]. Electrified technologies use electrons to drive reactions of interest. Electrons are deemed green chemicals when derived from renewable and clean sources of electricity. Therefore, electrocatalysis offers appealing advantages compared to the conventional physical and biochemical removal of pollutants [4,5].

Nitrate ($NO_3^-$) pollution is one of the top ten water quality violations worldwide [6,7]. The treatment of this challenging oxyanion is not trivial. Nitrate, as a ubiquitous contaminant, has been treated by centralized large-scale methods such as reverse osmosis, ion exchange, and bioremediation [8–11]. However, further treating brines and sludge from these approaches increases operational costs by more than 30 % [12]. In this context, electrochemistry may open new treatment avenues for sustainable management of nitrate pollution [13]. The electrochemical reduction of nitrate (ERN) has two main goal products depending on the control on selective transformation: nitrogen gas ($N_2$) and ammonia ($NH_3$). Product selectivity might be attained by controlling specific experimental conditions, particularly the choice of electrode material utilized [14–18] and the electrolyte composition [19,20]. For drinking water applications, the focus lies on the obtention of harmless $N_2$ gas [21]. However, recent efforts have concentrated on producing $NH_3$ as an added-value product [22,23] in line with ongoing efforts in the electrochemical reduction of nitrogen [24,25]. This resource recovery approach has become a hot topic in environmental research. Although this approach is in its infancy, the development of feasible applications is becoming more achievable by incorporating $NO_3^-$ pre-concentration systems, $NO_3^-$ conversion systems, and $NH_3$ recovery units.

Concerning $NO_3^-$ electro-conversion systems, current research focuses on identifying materials that exhibit high performance in $NO_3^-$ conversion and demonstrate superior selectivity toward $NH_3$ production [26–29]. While significant progress has been made in this aspect, fewer studies have concentrated on scaling this process for real-world applications. To align this approach on a large scale, several critical challenges must be addressed, including the utilization of free-standing electrodes [30], stability against inorganic scaling produced in real water matrices [31], designing suitable reactor configurations to maximize electrode utilization [32], and achieving high $NH_3$ yield (measured in mmol $NH_3$ $g^{-1}_{cat}$ $h^{-1}$ or mmol $NH_3$ $cm^{-2}_{cat}$ $h^{-1}$) [33]. In response to these essential requirements, open-pore metal foam electrodes have emerged as a promising and viable configuration to overcome these challenges. Metallic foams offer various advantages, including enhanced mass transport, excellent electrical conductivity, high electrochemical surface area, and adaptability to different reactor configurations compared to two-dimensional electrodes [34–36]. For instance, a comparison between Cu and Ni plate and foam electrodes performance after an identical amount of charge transferred during ERN electrolysis showed higher nitrate conversion (%), calculated using Equation 1, on Cu foam than on plate, but almost identical values were reached on Ni foam and plate electrodes, as indicated in Table 1.

$$Nitrate\ conversion\ (\%) = \frac{C_{NO_3^-,0}}{C_{NO_3^-,0} - C_{NO_3^-,t}} \times 100 \tag{1}$$

where $C_{NO_3^-,0}$ is the initial nitrate concentration (mg $NO_3^-$-N $L^{-1}$), and $C_{NO_3^-,t}$ is the nitrate concentration at time $t$ (mg $NO_3^-$-N $L^{-1}$).

Thus, the role of metal foams during the ERN may vary depending on their composition, which influences their characterization and activity evaluation. Metal foam applied for ERN can be classified into three types: *i*) active materials (such as Cu foam), *ii*) support materials (inactive current collectors, like Ni foam), and *iii*) modified materials (catalyst-supported electrodes, where foam electrodes—whether active or inactive—are fully or partially coated with an additional catalytic material, denoted as $Cu_{foam}$/M and $Ni_{foam}$/M, respectively).

4

**Table 1.** Comparison of ERN galvanostatic electrolysis results on Cu and Ni electrodes using plate and foam electrodes. Plate electrodes were evaluated at 20 mA cm$^{-2}$ during 90 min on 6.0 cm$^2$ electrodes (Q = 648 C). Initial solution composition: 100 mg L$^{-1}$ NO$_3^-$-N in 50 mM Na$_2$SO$_4$. Foam electrodes were evaluated at 40 mA cm$^{-2}$ during 120 min on 2.25 cm$^2$ electrodes (Q = 648 C). Initial solution composition: 30 mg L$^{-1}$ NO$_3^-$-N in 12.5 mM Na$_2$SO$_4$.

| Element | Electrode Configuration | Nitrate Conversion (%) |
|---|---|---|
| Cu | Plate [37] | 22 ± 2 |
| | Foam [38] | 55 ± 4 |
| Ni | Plate [37] | 8 ± 2 |
| | Foam [39] | 10 ± 2 |

Independently of the initial pH solution, the ERN mechanism yields hydroxide ions that increase solution pH, reaching in some instances values as high as pH 11. The solution alkalinization during ERN promotes the generation of oxides and hydroxides on the metallic electrode surface. Consequently, the coexistence of metal, oxide, and hydroxide sites on the foam electrode surface increases entropy and facilitates the provision of adsorption sites during ERN. Table 2 provides a summary of the bulk resistivity of various materials, including C, Ni, Cu, Cu-based oxides, Ni-based oxides, Al$_2$O$_3$, and SiO$_2$. These values underscore the exceptional electrical conductivity of Cu and Ni foams and exhibit much lower bulk resistivity (Ω cm) for passive Cu and Ni-based oxides than for insulating-type oxides such as Al$_2$O$_3$ and SiO$_2$. Therefore, the presence of Cu- and Ni-based oxides on the foam surface does not significantly impact the overall conductivity of the electrode. On the contrary, the presence of these oxides in small quantities can be advantageous for increasing the overall electrochemically active surface area (ECSA), number of adsorption sites, and electrode stability [40]. In fact, some studies suggest that these metal oxides may have higher electrocatalytic activity on the reduction of oxyanions [41–43].

122 **Table 2.** Bulk resistivity ($\Omega$ cm) of various materials considered as conductors, semiconductors,

123 and insulators.

| Material | Bulk resistivity ($\Omega$ cm) |
|---|---|
| Carbon foam* | $32.3 \times 10^{-2}$ |
| Nickel foam** | $6.9 \times 10^{-6}$ |
| Cu foam* | $65.2 \times 10^{-6}$ |
| $Cu_2O$[44] | $3.7 \times 10^{3}$ |
| CuO[44] | $1.1 \times 10^{3}$ |
| $NiO_x$[45] | $1.0 \times 10^{2} - 1.0 \times 10^{9}$ |
| $Ni(OH)_x$[46] | $1.0 \times 10^{5} - 1.0 \times 10^{6}$ |
| $Al_2O_3$[47] | $1.0 \times 10^{15} - 1.0 \times 10^{17}$ |
| $SiO_2$[47] | $1.0 \times 10^{14} - 1.0 \times 10^{16}$ |

124 *Values provided from the manufacturer: ERG Aerospace Corporation

125 **Values provided from the manufacturer: ATT Advanced elemental materials

126        This critical review delves into the fundamental parameters of three-dimensional (3D)

127 foam electrodes and underscores the importance of accurate interpretation for reporting ERN

128 performance. It looks into the multifaceted role of metal foams, exploring its functionality as an

129 active material, support material, and modified foam. The review encompasses pertinent

130 examples of 3D modified electrodes aimed at enhancing electrocatalytic performance in ERN,

131 along with a discussion of the most recent modification strategies. By presenting these materials,

132 the review offers an updated overview of the current state-of-the-art in this specialized research

133 domain. Furthermore, the review extends its perspective to the future by outlining potential

134 directions and identifying gaps that require attention for the further development of 3D foam-

135 based electrocatalysts in ERN applications.

136

## 2. Defining key characterization parameters of metal-based three-dimensional foam electrodes

Considering their distinctive features, 3D metal foam electrodes (e.g., Cu, Ni, Co, Al) have emerged as the primary substrate or active material for electrocatalysis in many fields [48–50]. The 3D configuration provides excellent electrical properties and a smart spatial configuration that results in outstanding ERN performance. The choice of conductive material depends on the role of the electrode during the ERN, which may be a support electrode, active electrode, or both [51–53]. This classification is determined by the electrocatalytic response of the pristine foams and modified materials in the presence of $NO_3^-$, as evidenced by the increase in current density, as illustrated in Figure 1. The most determining properties to characterize in these materials are pore per inch (*PPI*) and electrochemically active surface area (ECSA). These physical descriptors play a relevant impact in catalytic activity evaluation as they drive the comparisons in terms of mass transfer efficiency and applied current density ($j$, mA cm$^{-2}$), respectively.
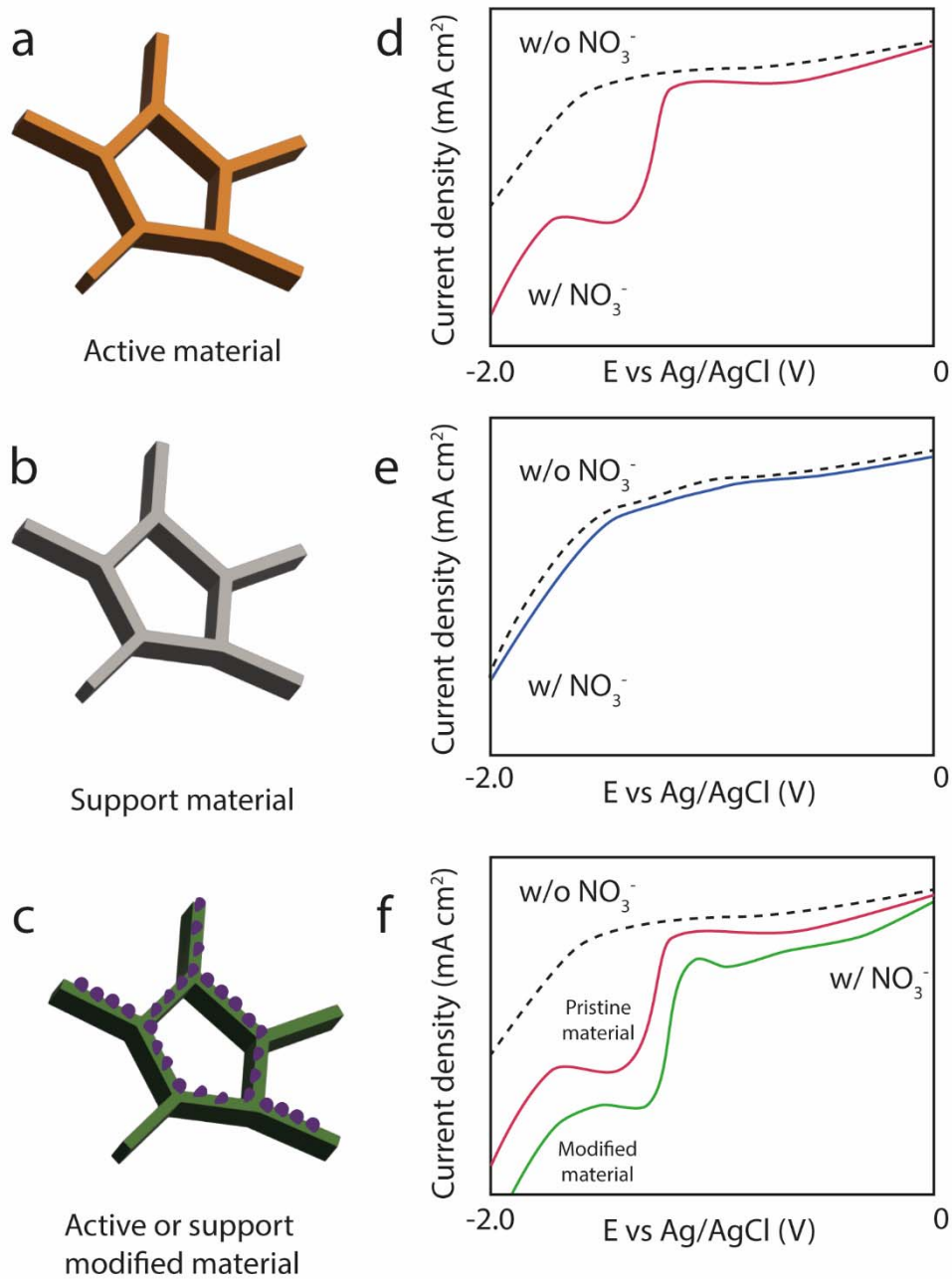
**Figure 1.** Classification of foam electrode: (a) active material, (b) support material, and (c) active or support modified material. Linear sweep voltammetry of (d) $Cu_{foam}$, (e) $Ni_{foam}$, and (f) $Cu_{foam}/Co(OH)_x$ conducted in $Na_2SO_4$ solution in absence and presence of $NaNO_3$ at 50 mV s$^{-1}$. Adapted from [17,38,39].

## 2.1    *On the relevance of emptiness: describing pore per inch (PPI)*

The *PPI* is a commonly overlooked but crucial parameter to characterize metal foam materials. The *PPI* refers to the number of pores present per linear inch of the foam structure, giving a direct average value of emptiness contained in the 3D structure [54]. The number of pores can indirectly indicate average pore size/diameter since smaller pores can be encapsulated with a higher density in a linear inch. Thus, higher *PPI* values are generally associated with notoriously smaller pore sizes and less efficient mass transfer. Therefore, the *PPI* value is essential for the possible implementation of 3D foam electrodes in flow-through and flow-by electrochemical reactor designs, as it controls the hydrodynamic behavior of solution flowing through the interconnected pores in the foam [55,56]. For instance, the electrochemical characterization of reactors (flow-through and flow-by) can be performed using the volumetric mass transport coefficient ($k_mA$) for a process controlled by mass transfer. This parameter, typically evaluated using the limiting current from a monoelectronic redox mediator in solution such as ferrocyanide ion over various electrolyte mean linear flow velocities, provides both mass transfer coefficient ($k_m$, m s$^{-1}$) and electroactive specific area ($A_s$, m$^{-1}$) properties in flow-by reactors [57–62]. The $k_mA$ (s$^{-1}$) is determined from the limiting current $I_L$ (A) according to Equation (2)

$$k_m A_s = \frac{I_L}{nFCV_c} \tag{2}$$

where $n$ is the number of electrons involved in the reaction ($n = 1$, considering the redox couple Fe(CN)$_6^{3-}$/Fe(CN)$_6^{4-}$), $F$ is the Faraday's constant (96485 C mol$^{-1}$), $C$ is the bulk concentration of Fe(CN)$_6^{3-}$ (mol m$^{-3}$), and $V_c$ is the active volume (m$^3$).

On the other hand, flow-through reactors can be also characterized using the $k_mA$ vs. $I_L$ relationship, according to Equation (3)

$$I_L = nFCuA_r \left[ 1 - e^{\left( -\frac{L k_m A_s}{u} \right)} \right] \tag{3}$$

180 where $n$ is the number of electrons involved in the electrochemical reaction, $u$ is the flow rate (m

181 $s^{-1}$), $A_r$ is the cross-sectional area ($m^2$), and $L$ is the thickness of the porous electrode (m) [63,64].

182 Figure 2 illustrates three Cu foams with increasing *PPIs* of 20, 40, and 110. The optical

183 images (Figures 2a, b, and c) clearly illustrate the polydisperse nature of interconnected pores and

184 the decreasing pore size distribution with increasing *PPI* number. Figures 2d, e, and f illustrate

185 the heterogeneous morphology of the pores by scanning electron microscope (SEM) at low

186 magnification (74X) and 5 keV. It can be observed that the average diameter of interconnected

187 pores decreases in size with increasing *PPI,* going from an average value of 1.55 mm at 20 *PPI*

188 down to 236 μm at 110 *PPI.*

189 In porous structures such as 3D metal foams, surface area ($cm^2$) can be normalized in two

190 distinct ways. Firstly, by areal density, which is related to the mass or amount of material ($cm^2 \ g^{-1}$

191 $^1$). Secondly, the specific surface area (SSA) is expressed relative to the volume of the 3D foam

192 ($cm^2 \ cm^{-3}$). Both parameters hold particular significance in electrocatalysis, where processes are

193 primarily driven by interfacial interactions. Notably, both areal density and *SSA* exhibit a linear

194 increase with rising *PPI.*

195 Furthermore, the inherent tortuosity of foams with varying *PPI* significantly affects reactants

196 and product mass transfer close to the foam surface. Higher *PPI* values lead to increased

197 tortuosity, impacting the renewal of reactant from the bulk solution and the accumulation of

198 products at the electrode surface. Conversely, lower *PPI* values can enhance mass transfer by

199 facilitating concentration equilibrium between interfacial and bulk solution species [65,66]. In

200 particular, the interfacial pH can drastically increase during ERN and differ from the bulk solution

201 pH depending on operational conditions. Thus, the *PPI* value impacts the magnitude and

202 extension of the solution alkalinization at the electrode surface. Subsequently, the local alkaline

203 pH can exacerbate additional issues in complex water matrices due to $Mg^{2+}$ and $Ca^{2+}$ ions,

204 resulting in inorganic scaling on the foam surface [31,67]. Consequently, different *PPI* values

205 may influence the decrease in ERN activity on the foam due to inorganic scaling on the electrode

206 surface.
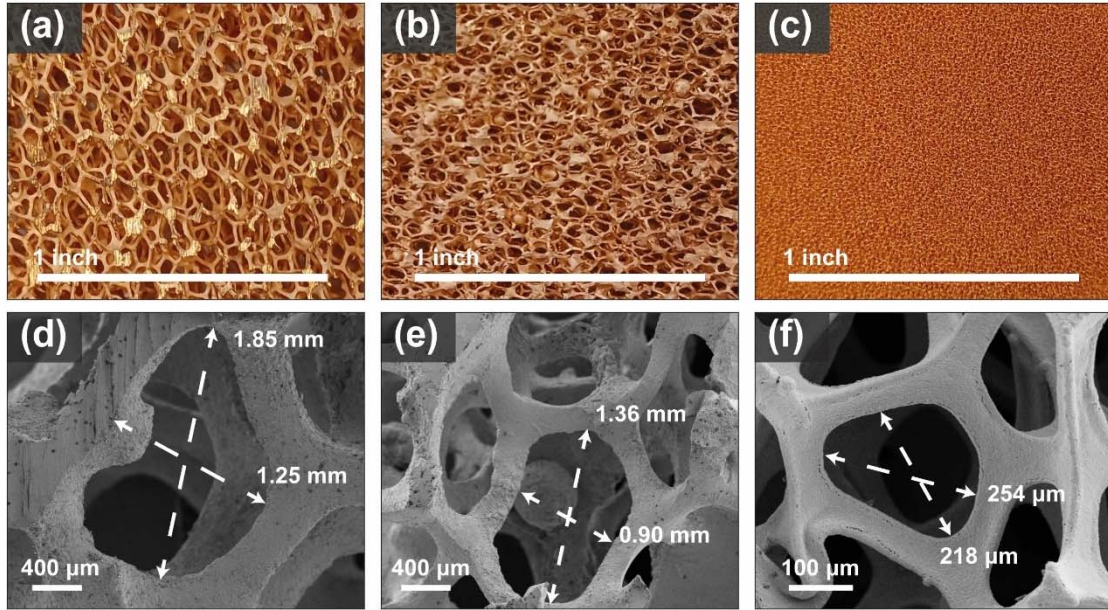
**Figure 2.** Cu foam at 20, 40, and 110 PPI at different conditions: (a, b, c) optical imagining, and (d, e, f) SEM images to determine surface morphology. Cu foam 20 and 40 *PPI* were acquired from ERG Aerospace Corporation and 110 *PPI* from Futt.

### *2.2    The interconnection of electrocatalytic response and the electrochemically active surface area (ECSA)*

For applications in electrocatalysis, the reactive surface area is one of the most important parameters. In the case of 3D metal foams, the actual electroactive surface area is significantly different from the geometrical area. Thus, the specific surface area of a foam is the amount of surface area within a given bulk volume of foam. Consequently, various methods have been employed to estimate this relevant parameter. One commonly used technique for surface area measurement in catalyst's characterization is the gas adsorption, which is based on argon (Ar), krypton (Kr) or nitrogen ($N_2$) gas physisorption on the solid catalyst at cryogenic temperature by the Brunauer-Emmett-Teller (BET) approach [68,69]. However, this *ex-situ* technique faces challenges when examining samples that are predominantly macroporous (i.e., metal foams with low *PPI*) with a lower surface area in comparison with meso- and micro- porous materials (e.g., zeolites, activated carbons, and metal organic frameworks (MOFs)). Notably, metal foam electrodes typically represent low surface area samples ($<1$ $m^2/g$), rendering $N_2$ physisorption

unsuitable for most cases. Alternatively, Kr physisorption at 77 K has been successfully employed for evaluating surface area in metal foam electrodes [70]. Furthermore, mercury porosimetry has proposed as an alternative approach to assess the size distribution and porosity of metal-based 3D electrodes [71]. Giving that metal foam electrodes operate within an electrochemical solid/liquid interface during ERN, estimating and comparing their ECSA, which may not necessary equivalent to the total surface area estimated by gas physisorption or other physical methods [51], represents a major point of attention to benchmark different studies.

The ECSA denotes the active surface area actually involved in the electrochemical process [40,51,72,73]. The larger the ECSA, the greater the number of active sites available for electrochemical reactions to occur, leading to enhanced reaction rates and improved efficiency in a shorter treatment time. Although 3D metal foam electrode substrates can play different roles (i.e., active material, support material, or modified material), the ECSA can be evaluated regardless of that role. Thus, different single or multi-component foam-based materials can be benchmarked as electrocatalysts by normalizing their electrochemical response via their corresponding ECSA. The ECSA should be determined for the actual electrode under study since the bare metal foam electrodes might either diminish or increase their ECSA after incorporating an additional catalytic material on top.

Although multiple methods have been suggested for determining ECSA [72], discrepancies and errors persist in electrocatalyst research and make the present discussion timely. A common flaw is the misuse of the Randles-Sevcik equation to evaluate the ECSA for 3D materials. Randles-Sevcik relies on the use of an outer-sphere redox mediator in solution (*i.e.* $K_3Fe(CN)_6$) to estimate ECSA. However, Randles-Sevcik is not applicable to the case of metal foam electrodes since this approach is only strictly pertinent for evaluating planar electrodes or those with semi-infinite diffusion [74]. Hence, when used to determine the ECSA of 3D materials, the results are unreliable and mainly correspond to the 2D geometric surface area evaluation.

The ECSA of 3D metal foam electrodes can be estimated instead from the double layer capacitance ($C_{dl}$) and the specific capacitance ($C_s$) values, according to Equation (4):

$$ECSA\ (cm^2) = \frac{C_{dl}}{C_s} \qquad (4)$$

252  where $C_{dl}$ represents the double layer capacitance (μF) obtained either from cyclic voltammetry

253  (CV) or electrochemical impedance spectroscopy (EIS); and $C_s$ the specific capacitance value (μF

254  cm$^{-2}$). The $C_s$ is generally defined for an ideal flat surface and depends on the nature of the catalyst

255  (metal or metal oxide), as well as the solution pH (alkaline or acid). Different $C_s$ values can be

256  found in the literature in the range from 20 to 80 μF cm$^{-2}$ [51,75], being in most cases around 40

257  μF cm$^{-2}$ for both Ni and Cu oxide in alkaline solution [40,51,73,75] and 20 μF cm$^{-2}$ for the case

258  of metallic Ni in alkaline solution [36]. Thus, ECSA comparison is only possible between similar

259  electrocatalysts evaluated under similar experimental conditions [72], which is the case of

260  comparing bare metal foam electrodes (Cu or Ni foams) and multi-component foam-based

261  electrodes (Cu$_{foam}$/M or Ni$_{foam}$/M electrodes) during ERN. Nevertheless, ECSA estimation

262  contains a significant range of uncertainty due to the wide dispersion in $C_s$ values. The use of

263  Equation (4) it is useful mainly for comparison purposes and not for obtaining absolute values

264  [72].

265  The formation of an electrical double layer (EDL) at the electrode-electrolyte interface is a

266  fundamental phenomenon in electrochemistry [76,77]. When an electrode is immersed in an

267  electrolyte solution, ions from the solution are attracted to the electrode surface due to electrostatic

268  forces. This phenomenon results in the formation of two layers of charge: one layer of ions

269  adsorbed onto the electrode surface (the inner Helmholtz plane) and another layer of oppositely

270  charged ions in the solution adjacent to the electrode surface (the outer Helmholtz plane). Under

271  the assumption that no Faradaic processes take place within this narrow potential range (i.e., no

272  electron transfer reactions involving redox electroactive species), the behavior of the double layer

273  resembles that of a capacitor. In other words, the electrode-electrolyte interface defined by the

274  double layer behaves like a capacitor.  Consequently, the estimated $C_{dl}$ is directly connected to the

275  ECSA, since an extended surface area facilitates increased ion adsorption, thus amplifying the

276  electrical double layer and its capacitance. The most common electrochemical approach to

277  estimate the $C_{dl}$ is based on capacitive current evaluation by CV as a function of scan rate in a

278    narrow non-Faradaic potential range, using Equation (5), which assumes an ideal capacitor

279    behavior [78].

$$C_{dl} = \frac{\Delta I / 2}{v} \qquad\qquad (5)$$

280    where $\Delta I/2$ (A) denotes the half-current difference between the anodic and cathodic currents at

281    central potential, and $v$ stands for the scan rate (V s$^{-1}$). The slope from the corresponding graphical

282    representation provides the $C_{dl}$ value.

283    Despite the seemingly direct calculation of ECSA from CV, the procedure requires

284    meticulous care. Several factors need consideration to obtain accurate $C_{dl}$ values, even for flat 2D

285    electrodes. For the case of 3D metal foam-based electrodes, the task becomes more complicated.

286    Essential aspects to be considered during the electroanalytical procedure include but are not

287    limited to the electrical connections, effects of trapped air, electrode wettability, and surface

288    tension. Note that several of these aspects are *PPI*-dependent. As reported by Morales *et. al*

289    several steps should be considered in order to obtained reliable ECSA values [79]. Figure 3 details

290    four main steps and electrochemical considerations essential for obtaining ECSA comparison

291    among electrocatalysts.

292    Step 1: Initially it is crucial to perform CV scans over a wide potential range to identify

293    regions where non-Faradaic current dominates and there is an absence of peaks or evidence of

294    Faradaic current. Neglecting this step could lead to an inaccurate depiction of capacitor

295    characteristics. As presented in Figure 3a, the non-Faradic region (enclosed by the green dotted

296    square) can be identified in the wide potential range. It is important to recognize that the specific

297    range varies based on the material electrochemical properties. Thus, it should be estimated in each

298    individual case. While many studies typically employ the open circuit potential (OCP) value as

299    the central potential, this approach is not universally applicable. For example, Cu foam presents

300    a Faradaic oxidation process in close proximity to the OCP in 0.1 mol L$^{-1}$ Na$_2$SO$_4$ [17]. Moreover,

301    when defining the range, it is essential to ensure that both cathodic and anodic currents overlap

302    in two subsequent potential scans, typically conducted within a window of 100 and 500 mV (see

303     Figure 3b). This overlapping also depends on the electrode material and the scanned potential

304     range.

305       Step 2: Researchers should optimize the data collection parameters since calculated

306     capacitance values are sensitive to variations of these parameters. While recording CV at different

307     scan rates, it is crucial for the operator to consider parameters such as current range and the size

308     of voltage step. Although the current range can be set either automatically or manually, it may

309     vary over several orders of magnitude depending on the range of scan rates employed. It is

310     advisable to assess the noise in the measurement by comparing results obtained at different current

311     range limits as presented in Figure 3c. An improper selection of the current range can introduce

312     significant noise into the measurements. Therefore, conducting separate experiments for each

313     scan rate, rather than using the same current range across both fast and slow scan rate, can be

314     beneficial. Additionally, careful selection of the voltage step size is essential, especially when

315     evaluations are carried out over a small range of 100 mV. Figure 3d shows the effect of choosing

316     an unsuitable voltage step on the data collection during the assessment. The voltage step affects

317     the CV profile near the upper and lower set potentials.

318       Step 3: Once the optimal data collection parameters have been identified, measurements

319     should be carried out spanning a broad range of scan rates (i.e., from 500 to 5 mV s$^{-1}$). While

320     higher scan rates might be applicable depending on the material being evaluated, slower rates can

321     be time-consuming and may not provide significant information about capacitance of the system.

322     Therefore, it is recommended to perform evaluations within the range of 250 to 5 mV s$^{-1}$ when

323     working with metal foams. Figure 3e presents a CV evaluation without considering the optimal

324     conditions, while Figure 3f denotes the CV performed at optimal conditions. Comparing both

325     graphs, a current underestimation was produced when the CV conditions were not optimized. The

326     improperly optimized parameters result in a CV profile with sharpened extremes, current noise,

327     and lower current compared to the reference dotted line. Conversely, under optimized parameters,

328     the CV profiles exhibit well-defined extremes, no evidence of noise within the selected current

329     range, and higher current compared to the same reference dotted line.

15

330        Step 4 - Once the data are collected, the analysis can be undertaken by considering the

331 cathodic current intensity, anodic current intensity, or the average of these two currents. The

332 capacitance values are calculated as mentioned, using Equations (4) and (5). Figure 3g presents a

333 comparison of capacitance values calculated using non-optimized and optimized conditions at

334 different potential ranges. It is noteworthy that under non-optimized conditions, the calculated

335 capacitance underestimates the system capacitance, whereas under optimized conditions, the

336 capacitance is 1.6 times higher than non-optimized conditions. Hence, determining the ECSA

337 appropriately is crucial for comparing electrocatalysts. It is important to realize that each material

338 requires unique conditions, and ECSA should be reported by the most appropriate evaluation.
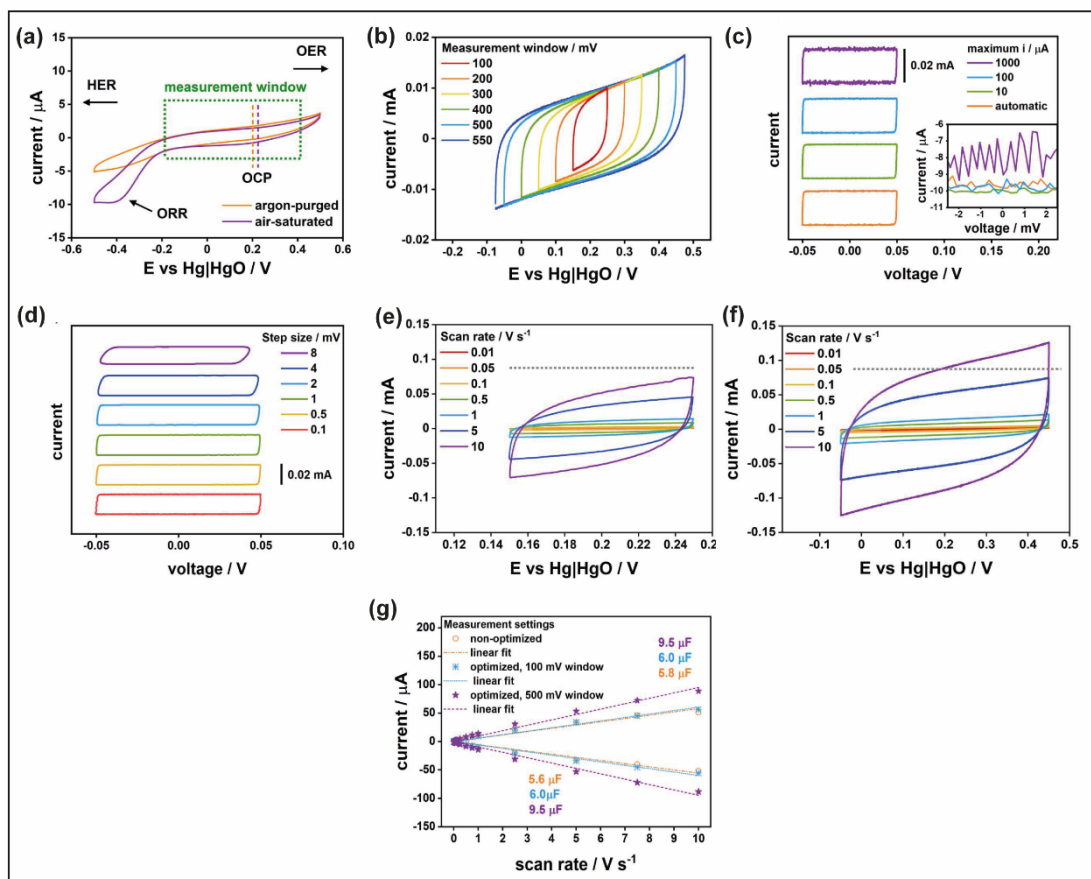


339

340 **Figure 3.** (a) Cyclic voltammetry of an electrochemical cell at 10 mV s$^{-1}$ to identify measurement

341 window. (b) Cyclic voltammetry at 500 mV s$^{-1}$ considering different measurement windows. (c)

342 Resistor-capacitor circuit evaluated at different maximum current parameter values and (d)

343 evaluation of the step size in the data collection RC-circuit. Evaluation of ECSA by CVs under

344    (e) non-optimized and (f) optimized electrochemical parameters. (g) Capacitance values obtained

345    under different conditions. All measurements were performed in an argon-purged 0.1 mol L$^{-1}$

346    NaOH aqueous solution. Figures adapted from [79] (CC-BY 4.0 - IOP Publishing).

347       The EIS is an alternative electroanalytical technique to estimate ECSA from $C_{dl}$. In particular,

348    EIS exhibiting capacitive current in the high frequency domain allows to evaluate the interfacial

349    capacitance. The interfacial capacitance simultaneously embraces the $C_{dl}$ contribution and the

350    capacitance associated with the oxide and/or hydroxide layer formed on some metallic surfaces

351    during ERN. This inclusion is relevant in the case of metallic foams such as Cu and Ni, as it is

352    commonly reported the formation of oxide/hydroxide layers. This type of complex metal-oxide-

353    electrolyte interface is not fully described by an ideal capacitor behavior and requires the use of

354    a constant phase element (CPE). The CPE is a mathematical element that helps to fit the

355    equivalent circuit and account for the distribution of dielectric properties of the interface [78].

356    Typically, after EIS assessment at potentials on the capacitive current domain in a frequency range

357    from 100 kHz to 0.01 Hz, either graphical analysis is performed [80] or an equivalent circuit is

358    modeled and fitted to the EIS data after solution resistance ($R_s$) correction. The simplest and most

359    common equivalent circuit involves the $R_s$, the charge transfer resistance ($R_{ct}$), and a CPE

360    representing the double layer capacitance. The frequency-dependent impedance ($Z$) for a CPE is

361    defined by Equation (6).

$$Z_{(\omega)} = \frac{1}{Q(i\omega)^{\alpha}} \tag{6}$$

362    where $Z$ is the impedance in $\Omega$ cm$^{-2}$, $i$ is the imaginary part of the complex number, and $\omega$ the

363    angular frequency in rad s$^{-1}$. The parameters related to the CPE are $Q$ and $\alpha$ ($1 \geq \alpha \geq 0$), which are

364    determined from the equivalent circuit fitting and are independent of the frequency. If $\alpha = 1$ the

365    CPE is a capacitor and $Q$ is the $C_{dl}$ and if $\alpha = 0$ the CPE is a resistor and $Q$ is the resistance.

366    Meanwhile, the $C_{dl}$ when $\alpha \neq 1$ and $\geq 0.7$ can be estimated by Equation (7) [81,82].

$$C_{dl} = \left[ Q \left( \frac{1}{R_s} + \frac{1}{R_{ct}} \right)^{\alpha-1} \right]^{1/\alpha} \tag{7}$$

17

367　　　Various studies in the literature have compared ECSA values ascertained from CV and EIS,

368　　attempting to gauge the accuracy of each technique given significant differences that oscillate

369　　between ±15 % and ±40 % [40,75,79,82,83]. In studies evaluating different electrode

370　　compositions or modified materials, both CV and/or EIS can be applicable without preference, if

371　　comparison is conducted under similar experimental conditions. Regarding equipment

372　　capabilities, the CV approach is basic and simpler compared to EIS, which requires a specific

373　　module and further specialized data treatment. However, a comprehensive evaluation of 3D foam-

374　　based electrodes is still lacking, leaving unresolved the question of the preferred method in such

375　　scenarios.

376　　Estimating the ECSA is an important step to benchmark electrocatalytic performance of 3D

377　　electrodes. The ECSA and the *PPI* value play a relevant role to ascertain an accurate activity

378　　evaluation under identically comparable current density. In order to enable direct benchmarking

379　　of electrocatalysts for ERN, authors should provide reliable metrics normalized by the

380　　electroactive area of the material in consideration. When considering the $NH_3$ yield from ERN,

381　　outcomes are barely reported in intrinsically comparable intensive metrics. A few articles that

382　　encompass the use of such relevant metrics for direct benchmarking report drastically different

383　　key indicator parameters such as the catalytic activity per mass or the catalytic activity per surface

384　　area. It is important to remark that in the case of 3D foam-based electrodes, where the mass of the

385　　active material might be difficult to estimate, the intrinsic electrocatalytic activity normalized and

386　　compared using the ECSA seems to be a more suitable approach to enable transparent and direct

387　　comparison between electrocatalyst development outcomes in literature. While the ECSA can be

388　　used for comparison between electrocatalyst, the use of 3D metal foam in flow-through or flow-

389　　by reactors for ERN under mass transfer conditions should be evaluated using the $k_mA$ parameter

390　　to account for dimensional and structural differences between electrode configurations [63]. By

391　　combining the ECSA or the geometrical 3D area, the mass transfer coefficient can be estimated

392　　and compared between the two area determination approaches. Comparisons between electrodes

393 with different PPI values should be performed under the same hydrodynamic pattern (flow-
394 through or flow-by reactors) to clearly establish the benefits on mass transfer parameters.

**3. Understanding differences between scaffolds and active supports: Selected examples**

395

396 **of novel modified foam-based electrocatalysts for ERN (Cu$_{foam}$/M and Ni$_{foam}$/M)**

397 The rational design of electrocatalysts often prioritizes the use of earth-abundant materials,

398 either in bulk or nano-enabled configurations, to minimize electrode capital costs. While platinum

399 group materials (PGMs) are well-known for their exceptional catalytic performance, their high

400 cost and scarcity limit their usage to ultra-low content or single-atom configurations [37,84].

401 Consequently, most bulk metal-based 3D electrodes discussed in the literature predominantly

402 feature earth-abundant metals such as Cu and Ni. The mechanisms and fundamentals of ERN on

403 those materials have been thoroughly discussed in several review articles [14,85–87]. In contrast,

404 the benchmarking of ERN based on robust self-standing Cu- and Ni-based electrodes has been

405 seldom explored. Thus, this section reviews some selected studies from the literature that used

406 either active or scaffold modified materials (Cu$_{foam}$/M and Ni$_{foam}$/M) as electrodes for the ERN.

407 The modification of Cu and Ni foam electrodes has been mainly reported using two

408 techniques: electrodeposition and solvothermal method. Electrodeposition, a well-established

409 electrochemical technique, which utilizes a metal precursor in solution along with a supporting

410 electrolyte and/or additives to control deposit characteristics. Electrodeposition is typically

411 employed on flat electrode surfaces due to the homogeneity of the formed deposit. However,

412 electrodeposition on 3D metal foam electrodes results in the formation of heterogeneous deposits

413 across the thickness of the foam due to mass transfer limitations of the reactant within its 3D

414 structure. In contrast, this synthetic approach facilitates *in-situ* nucleation and growth of the

415 deposited active material, thereby providing an enhanced attachment to the foam substrate.

416 Another commonly reported technique for modifying foam electrodes is the solvothermal

417 approach, which involves crystal nucleation and growth under moderate to high temperature (100

418 – 1000 ºC) and pressure (1 – 100 atm) conditions within a steel pressure vessel. In this case as

419 well, solvent, metal precursor concentration, additives, and reaction time play all a significant

19

420  role in the synthesis. Moreover, the synthesized material is formed and deposited on the foam

421  electrode, as well as on the solution. A direct comparison between these two electrode

422  modification techniques has shown that electrodeposited materials exhibit higher mechanical and

423  chemical stability than those deposited by solvothermal methods [88,89]. However, the total

424  loading and distribution of the synthesized material by electrodeposition through the 3D structure

425  of the foam significantly vary, reaching a more homogeneous distribution by the solvothermal

426  deposition method. This fact may directly impact the type of reactor configuration selected for

427  ERN. The flow-by configuration is well-adapted for modified foam electrodes synthesized by

428  electrodeposition because only a narrow part of the total thickness of the foam electrode

429  participates directly in the ERN, which is the one mainly containing the added material. In

430  contrast, the flow-through configuration is well-adapted for more homogenous electrodes

431  synthesized by the solvothermal deposition method because the whole thickness of the foam

432  electrode participates in the ERN.

433  Figure 4a illustrates a typical experimental setup for electrodeposition on foam electrodes,

434  featuring a three-electrodes electrochemical cell comprising a reference electrode (e.g., Ag/AgCl,

435  saturated calomel electrode (SCE)), a counter electrode (e.g., Pt plate, dimensionless stable

436  anode), and a working electrode (e.g., Ni or Cu foam). As depicted in Figure 4a, different solution

437  compositions can be employed to obtain various modified materials, with electrodeposition times

438  typically within a few minutes for nanoparticles deposition. In particular, this example illustrates

439  the modification of Cu foam by adding $Cu_2O$, $Ni(OH)_2$, $SnO_2$, or $Co(OH)_x$ [90]. Figure 4b depicts

440  the hydrothermal approach for modifying Cu foam, involving a pre-treatment to oxidize the Cu

441  foam surface followed by a hydrothermal step using a solution of $KMnO_4$ at 180 °C for 2.5 h.

442  Compared to electrodeposition, hydrothermal procedures of synthesis involve higher temperature

443  and longer reaction times, typically in the range of a few hours for superficial modification. Figure

444  4c shows a SEM image of $Cu_{foam}/Co(OH)_x$ obtained by electrodeposition, exhibiting the

445  coexistence of Cu and $Co(OH)_x$ nanodomains on the electrode surface. Figure 4d presents a

446  transmission electron microscope image illustrating the solid-solid interface between $MnO_2$

447     particles obtained by hydrothermal treatment and previously generated CuO on the surface of Cu

448     foam.

449        In the subsequent sections, some selected studies on modified Cu and Ni foam electrodes are

450     addressed to demonstrate the lack of standardization reporting ERN performance at present and

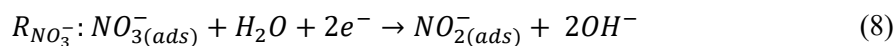451     some gaps in this research field are highlighted.
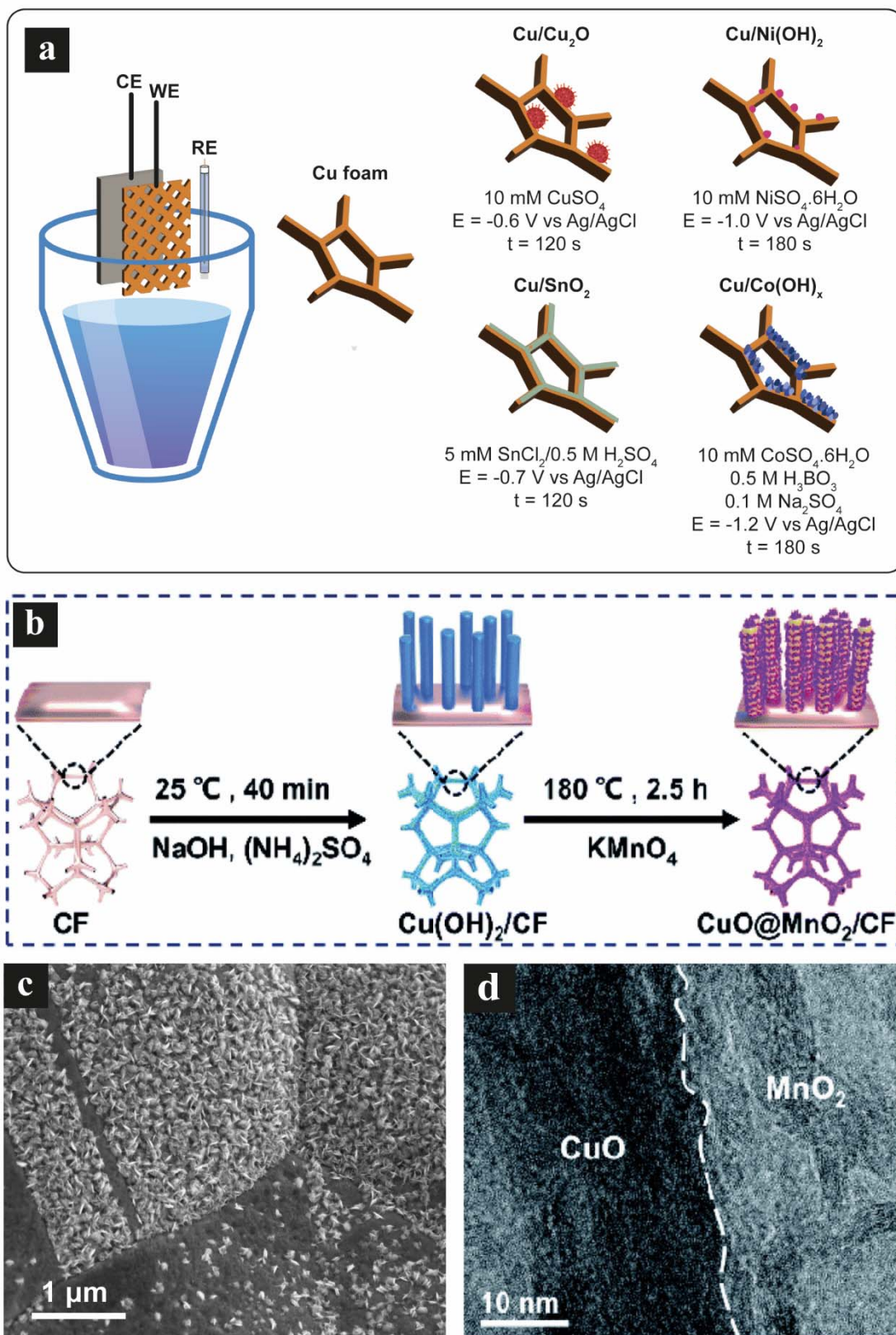
**Figure 4.** (a) Sketch of experimental conditions considering electrolyte, applied potential, and time for electrodeposition of bimetallic electrodes using Cu foam as self-standing active

material [90]. (b) Sketch of Cu foam modification with $Cu(OH)_2$ and hydrothermal procedure to obtain $CuO@MnO_2/CF$ [91]. (c) Scanning electron microscopy image of $Cu/Co(OH)_x$ prepared by electrodeposition [90]. (d) High resolution transmission electron microscopy images of $CuO@MnO_2/CF$ [91].

### 3.1. Modified copper foam as an active material for ERN

Copper and copper-based materials are well-recognized catalysts in ERN for facilitating the conversion of $NO_3^-$ to $NO_2^-$. Cu foam is a self-standing electrode material classified as type *i)* active material, which plays both roles as an active catalyst and support material. Thus, Cu foam partially contributes to the ERN electrocatalytic response in $Cu_{foam}/M$ modified materials acting as electrocatalysts for ERN. Cerrón-Calle *et al.* reported the electrochemical behavior of bare Cu foam in the presence of a $NaNO_3$ solution at different concentrations to identify the characteristic reduction peaks associated with the mechanistic steps in ERN [38]. As presented in Figure 5a, the oxidation (O1) and reduction (R1 & R2) peaks associated with Cu surface modifications taking place at the electrode surface do not increase in current when the $NO_3^-$ concentration in solution increases. Meanwhile, the cathodic current displayed at more negative potential than -0.15 V vs RHE increases with the concentration of $NO_3^-$ in the solution. Furthermore, Figure 5b demonstrates by linear sweep voltammetry the separated contributions from $NO_3^-$ reduction to $NO_2^-$ (at -0.4 V vs RHE) and the further reduction of $NO_2^-$ to $NH_3$ (at -1.0 V vs RHE), according to Equations (8) and (9), respectively.

$$R_{NO_3^-}: NO_{3(ads)}^- + H_2O + 2e^- \rightarrow NO_{2(ads)}^- + 2OH^- \tag{8}$$

$$R_{NO_2^-}: NO_{2(ads)}^- + 5H_2O + 6e^- \rightarrow NH_3 + 7OH^- \tag{9}$$

The electrochemical characterization of pristine Cu foam underscores its potential to reduce $NO_3^-$ to $NH_3$ directly in Cu foam without any additional modification. However, the main drawbacks of Cu-based materials for ERN are $NO_2^-$ accumulation and low kinetic constants. To mitigate $NO_2^-$ accumulation, modifying Cu foam with additional active materials to react synergistically in both reactions, Equations (8) and (9), have been extensively explored. Table 3 presents some selected examples of recent studies utilizing modified Cu foam electrodes,

including experimental conditions and key performance parameters for activity and selectivity evaluation. Additionally, Table 3 includes the ERN electrolysis results obtained by pristine Cu foam electrodes under identical experimental conditions in each case. This allows to evaluate the real impact of the modification incorporated into the electrode by subtracting the participation of the bare Cu foam electrode. In particular, only modified Cu foam materials where several consecutive cycles of electrolysis were performed to evaluate the catalyst stability are highlighted in Table 3. For example, $Cu_{foam}$/Pt [38] and $Cu_{foam}$/Co(OH)$_x$ [17] electrocatalysts are compared under galvanostatic conditions with the bare Cu foam and provide a superior $NO_3^-$ conversion, ammonia selectivity ($S_{NH3}$) and faradaic efficiency ($FE_{NH3}$) 21-22%, as shown in Table 3. Alternatively, Changhui Zhou *et al.* described the modification of Cu foam by generating $Cu(OH)_2$ nanowires on its surface, thereby increasing the surface area available for adsorption and conversion of $NO_3^-$ to $NO_2^-$ [92]. In addition to this, to boost the $NH_3$ generation, Pd sites were incorporated as atomic hydrogen sources to achieve further reduction beyond $NO_2^-$. Figure 5c illustrates the synergetic impact of these two combined modifications on the $NO_3^-$ conversion profile during ERN, since neither the increase in surface area produced by $Cu(OH)_2$ nanowires, nor the presence of Pd on bare Cu foam electrodes, provide the nitrate removal efficiency reached by $Cu_{foam}$/Cu(OH)$_2$/Pd electrodes. It is proposed that the incorporation of Pd sites consume the $NO_2^-$ produced by Cu sites, freeing up sites and accelerating the overall reaction [92]. This is clearly highlighted in Table 3, where $NO_3^-$ conversion by potentiostatic electrolysis reaches 100% and $S_{NH3}$ 98.8% on $Cu_{foam}$/Cu(OH)$_2$/Pd electrodes, meanwhile bare Cu foam gets blocked by the rate-limiting step reaction, Equation (8), at 60% $NO_3^-$ conversion and 27% $S_{NH3}$. Moreover, this study proposes the complete removal of N from the solution by generating active chlorine species during electrolysis by adding NaCl in solution and using an undivided cell. This approach converts $NO_3^-$ into $NH_3$ and then in $N_2$ by homogeneous reaction of $NH_3$ and active chlorine species [15]. The approach of exploiting chemical conversion of $NH_3$ to $N_2$ has been also explored by other studies shown in Table 3 [93,94]. In another recent study, Wenyang Fu *et. al.* evaluated the selectivity of ERN on Cu foam modified with electrodeposited CoO in a high conductivity solution (0.4 M $Na_2SO_4$) containig 40 mM of $NO_3^-$ [95]. The results of the corresponding

508  potentiostatic electrolysis are shown in Table 3 and demonstrate a net enhanced performance on

509  $Cu_{foam}/CoO$ electrodes with respect to bare Cu foam. The modified electrodes display 87.6% $NO_3^-$

510  conversion, 97.3% $S_{NH3}$ and 96.7% $FE_{NH3}$. Moreover, the same modification based on CoO

511  electrodeposition is applied on Cu and Ni foams to compare them. Figure 5d compares the

512  evolution of $S_{NH3}$ during ERN for bare Cu foam, $Cu_{foam}/CoO$, as well as $Ni_{foam}/CoO$ electrodes,

513  being clearly demonstrated in this case that the synergetic effect produced by combining CoO

514  with Cu foam is much more relevant than the one displayed by CoO with Ni foam [95]. The

515  $Cu_{foam}/CuO@MnO_2$ [91] and $Cu_{foam}/Cu_3P$ [96] electrocatalysts have been also evaluated for ERN

516  by potentiostatic electrolysis exhibiting in both cases an enhanced performance in comparison

517  with Cu foam.
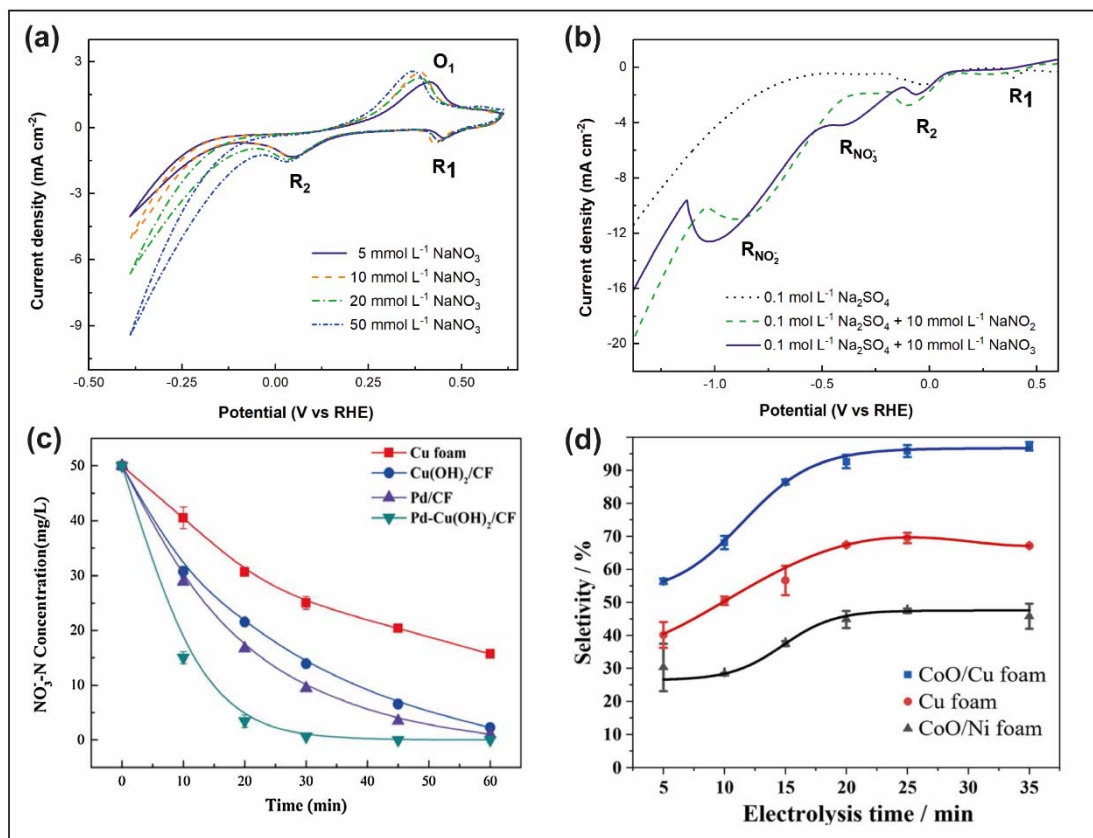


519  **Figure 5.** (a) Cyclic voltammetry at 10 mV s$^{-1}$ of Cu foam at different NaNO$_3$ concentration: 5,

520  10, 20, and 50 mmol L$^{-1}$. (b) Linear sweep voltammetry at 10 mV s$^{-1}$ of Cu foam in presence of

521  0.1 mol L$^{-1}$ Na$_2$SO$_4$ support electrolyte and with the presence of 10 mmol L$^{-1}$ of NaNO$_3$ or NaNO$_2$

522  [38]. (c) NO$_3^-$-N concentration evolution during ERN electrolysis on different Cu foam modified

523     materials. Experimental conditions: 50 mg $L^{-1}$ $NO_3^-$ at -1.2 V vs Ag/AgCl for 60 min [92]. (d)

524     $NH_3$ selectivity evolution during ERN electrolysis on Cu and Ni foam modified electrodes.

525     Experimental conditions: 0.4 mol $L^{-1}$ $Na_2SO_4$, 0.04 mol $L^{-1}$ $NO_3^-$ at -1.2 V vs Ag/AgCl for 35 min

526     [95].

527 **Table 3.** Some selected examples of modified Cu foam electrodes for ERN applications.

| Electrode | PPI | Area (cm²) | Experimental Conditions | NO₃⁻ conversion (%) | $S_{NH3}$ (%) | $FE_{NH3}$ (%) | Stability > 90% | Ref |
|---|---|---|---|---|---|---|---|---|
| Cu foam | 110 | $A_G$ = 2.25 *$A_{ECSA}$ = 1.2 m² | [Na₂SO₄] = 12.5 mM [NO₃⁻] = 2.1 mM $j$ = 40 mA cm⁻² | 55 | 55.3 | 11 | - | [38] |
| Cu$_{foam}$/Pt | 110 | $A_G$ = 2.25 | Time = 2 h Q = 648 C Undivided cell | 94 | 84.0 | 22 | 5 cycles | |
| Cu foam | - | $A_G$ = 4.0 | [Na₂SO₄] = 50 mM [NO₃⁻] = 2.1 mM [NaCl] = 70 mM | 2.6 | - | - | 5 cycles | [93] |
| Cu$_{foam}$/Cu nanobelt | - | $A_G$ = 4.0 | E = -1.4 V vs Ag/AgCl Time = 2 h Undivided cell | ≈100 | - | - | 5 cycles | |
| Cu foam | - | $A_G$ = 4.0 | [Na₂SO₄] = 50 mM [NO₃⁻] = 3.6 mM E = -1.2 V vs Ag/AgCl | 61.8 | 20 | 12.9 | - | [96] |
| Cu$_{foam}$/Cu₃P | - | $A_G$ = 4.0 | Time = 5 h Q = 900 C Undivided cell | 97.7 | 82.7 | 26.2 | 8 cycles | |
| Cu$_{foam}$/CuO | - | $A_G$ = 2.0 | [K₂SO₄] = 50 mM [NO₃⁻] = 14.3 mM E = -1.3 V vs SCE | 91.4 | 84.8 | 83.1 | - | [91] |
| Cu$_{foam}$/CuO@MnO₂ | - | $A_G$ = 2.0 *$A_{ECSA}$ = 465.2 | Time = 2 h Divided cell | 99.4 | 96.7 | 94.9 | 5 cycles | |
| Cu foam | ≈100 | $A_G$ = 6.0 | [Na₂SO₄] = 50 mM [NO₃⁻] = 0.8 mM [NaCl] = 0.1 M | 60 | 27.0 | | - | [92] |
| Cu$_{foam}$/Cu(OH)₂/Pd | ≈100 | $A_G$ = 6.0 | E = -1.2 V vs Ag/AgCl Time = 0.75 h Undivided cell | ≈100 | 98.8 | | 4 cycles | |
| Cu foam | - | $A_G$ = 6.0 **$A_{ECSA}$ = 18.6 | [Na₂SO₄] = 0.4 M [NO₃⁻] = 40 mM E = -1.2 V vs Ag/AgCl | 33.9 | 67.1 | 72.4 | - | [95] |
| Cu$_{foam}$/CoO | - | $A_G$ = 6.0 **$A_{ECSA}$ = 245 | Time = 0.58 h Undivided cell | 87.6 | 97.3 | 96.7 | 10 cycles | |
| Cu foam | - | $A_G$ = 12.0 | [Na₂SO₄] = 50 mM [NO₃⁻] = 7.15 mM | 24.3 | - | - | - | [94] |

| | | | | | | | | |
|---|---|---|---|---|---|---|---|---|
| $Cu_{foam}/Fe$ | - | $A_G = 12.0$ | $j = 25$ mA cm$^{-2}$<br>Time = 1.5 h<br>$Q = 1620$ C<br>Undivided cell | 98.6 | - | - | 8 cycles | |
| Cu foam | 110 | $A_G = 4.5$<br>*$A_{ECSA} = 1.7$ m$^2$ | [Na$_2$SO$_4$] = 12.5 mM [NO$_3^-$] = 2.1 mM<br>$j = 20$ mA cm$^{-2}$ | 55.3 | 68 | 11 | - | [17] |
| $Cu_{foam}/Co(OH)_x$ | 110 | $A_G = 4.5$<br>*$A_{ECSA} = 1.2$ m$^2$ | Time = 2 h<br>$Q = 648$ C<br>Undivided cells | 98.7 | 81 | 21 | 5 cycles | |

528    *ECSA calculated using the specific capacitance 40 µF cm$^{-2}$

529    **ECSA calculated using the specific capacitance 60 µF cm$^{-2}$

530

*3.2. Modified nickel foam as active material for ERN*

532		Electrodes based on Ni foam materials represent another type of metal-based 3D electrodes

533		(type *ii*), primarily serving as support material or inactive current collector. Unlike Cu foam

534		materials, Ni materials lack significant electrocatalytic activity for ERN. Consequently, the ERN

535		performance of bare Ni foam electrodes is seldom reported in the literature. As studied by

536		Xiangdong Tan *et al.*, [97], Figure 6a and Figure 6b depict the CV of bare Ni foam evaluating the

537		electrochemical response of this material in the absence and the presence of $NO_3^-$, respectively.

538		There is not a significant difference in current density when comparing both CV, which

539		demonstrates the low electrocatalytic activity of Ni foam for ERN. Thus, the role for Ni foam is

540		to serve as a scaffold material and facilitate the evaluation of other electrocatalytic materials on

541		its surface [97]. Figure 6c illustrates the electrocatalytic behavior of various modified Ni foam

542		electrodes ($Ni_{foam}$/M). In particular, $Ni_{foam}$/Cu and $Ni_{foam}$/Cu-Ni electrodes significantly improved

543		kinetics for ERN. This is attributed to the intrinsic activity of these electrodeposited materials and

544		not to the Ni foam itself [97]. This study also studies the complete removal of N from the solution

545		by generating active chlorine species during electrolysis by adding NaCl in solution and using an

546		undivided cell. This approach significantly improves the $N_2$ selectivity and has been also explored

547		by other studies shown in Table 4. In particular, Jianan Gao *et al.*, [86] obtained 100% $N_2$

548		selectivity in the presence of 2500 mg $L^{-1}$ $Cl^-$ in solution. Some selected examples of recent studies

549		utilizing modified Ni foam electrodes are presented in Table 4, including experimental conditions

550		and key performance parameters for activity and selectivity evaluation. In particular, modified Ni

551		foam materials where several consecutive cycles of electrolysis were performed to evaluate the

552		catalyst stability are highlighted in Table 4. For example, a recent study by Cerron-Calle *et al.*

553		evaluated electrodeposition of Cu and Co sites separately or combined on Ni foam as a strategy

554		to obtain modified $Ni_{foam}$/M electrodes exhibiting a relevant effect on ERN activity and selectivity

555		in several cases. Figure 6d showcases the electrolysis results on $Ni_{foam}$/$Cu_2O$/$Co(OH)_x$ electrode,

556		highlighting the high $NO_3^-$ conversion and $NH_3$ production achieved [39], which are almost

557		identical to the results displayed by $Cu_{foam}$/Pt electrode under identical experimental conditions

for ERN [38]. This is clearly pointed out by comparing their corresponding results reported in Tables 3 and 4. In particular, the $FE_{NH3}$ 22% and the $NO_3^-$ conversion >90% are equivalent in both cases, only a slightly higher $S_{NH3}$ 94% on $Ni_{foam}/Cu_2O/Co(OH)_x$ electrode (Table 4) than on $Cu_{foam}/Pt$ electrode ($S_{NH3}$ 84%, Table 3) is reported. Thus, it is demonstrated that type *iii)* modified electrode materials either based on Ni or Cu foam allow both to increase the ERN activity and direct its selectivity towards $NH_3$ production in the same magnitude. Moreover, Table 4 includes other types of $Ni_{foam}/M$ electrocatalysts such as those based on the pyrolysis of MOF [98], as well as those based on the addition of non-metallic elements such as P ($Ni_{foam}/NiCoP$ [99] and $Ni_{foam}/CoP$ nanowire array [100], S ($Ni_{foam}/NiCo_2S_4$ [101]) or B ($Ni_{foam}/Ni-BO_x$ [102]). The presence of a non-metallic element in addition to metals in the ERN electrocatalyst is demonstrated to produce a significant enhancement in $NO_3^-$ conversion, $S_{NH3}$ and $FE_{NH3}$ as is shown in Table 4.
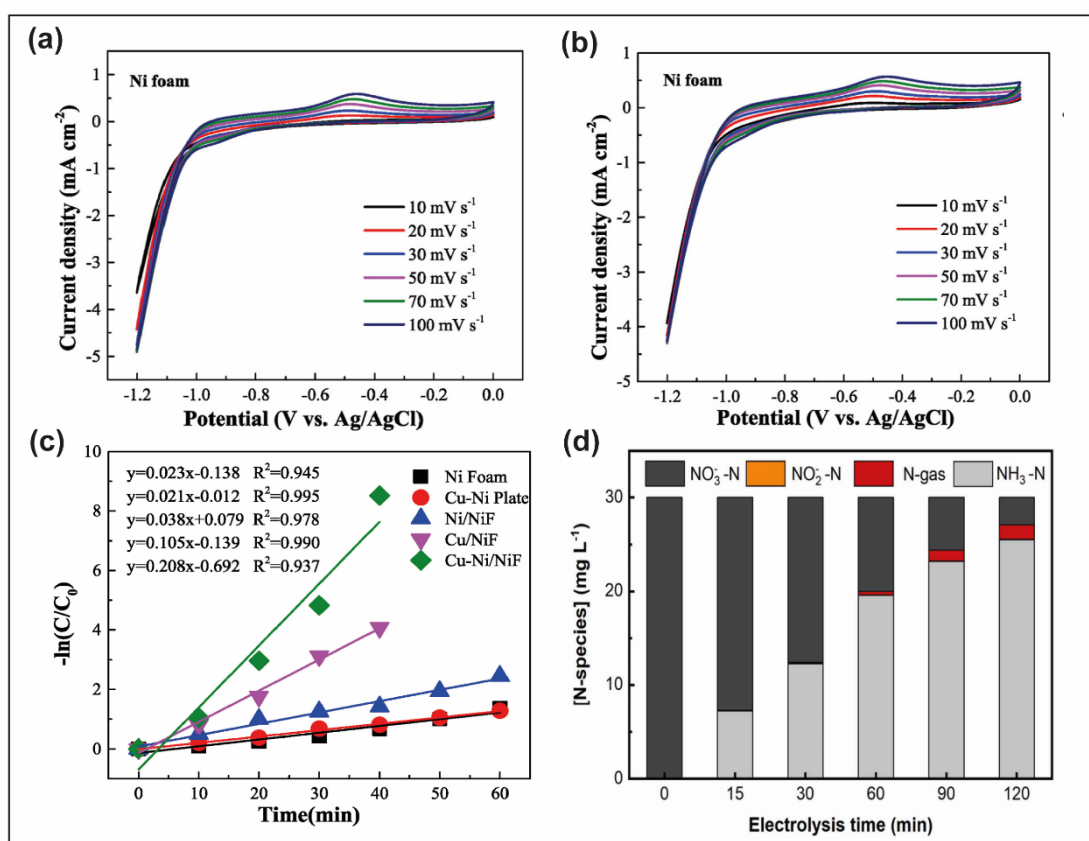


**Figure 6.** Cyclic voltammetry of Ni foam at different scan rate in (a) absence and (b) presence of 100 mg $L^{-1}$ $NO_3^-$-N in solution. (c) Pseudo-first order kinetic constants for ERN on different Ni

573    foam-based electrodes [97]. (d) $NO_3^-$-N conversion and products evolution during ERN

574    electrolysis using $Ni_{foam}/Cu_2O/Co(OH)_x$. Experimental conditions: 30 mg $L^{-1}$ $NO_3^-$-N and 12.5

575    mM $Na_2SO_4$ solution at 40 mA $cm^{-2}$ for 120 min [39].

576

577    Table 4. Some selected examples of modified Ni foam electrodes for ERN applications.

| Electrode | PPI | Area (cm²) | Experimental Conditions | NO$_3^-$ conversion (%) | S$_{NH3}$ (%) | FE$_{NH3}$ (%) | Stability > 90% | Ref |
|---|---|---|---|---|---|---|---|---|
| Ni$_{foam}$/P-doped-Co$_3$O$_4$ | - | A$_G$=8<br>**A$_{ECSA}$ = 1008 | [Na$_2$SO$_4$] = 50 mM [NO$_3^-$] = 3.6 mM<br>$E$ = -1.3 V vs SCE<br>Time = 2 h<br>Undivided cell | 98 | 78 | 31.4 | 10 cycles | [86] |
| Ni foam | 110 | A$_G$ = 2.25<br>*A$_{ECSA}$ = 1913 | | 9.6 | 95.8 | 2 | - | |
| Ni$_{foam}$/Cu$_2$O | 110 | A$_G$ = 2.0<br>*A$_{ECSA}$ = 4838 | [Na$_2$SO$_4$] = 12.5 mM [NO$_3^-$] = 2.1 mM<br>$j$ = 40 mA cm$^{-2}$<br>Time = 2 h<br>$Q$ = 648 C<br>Undivided cell | 28.4 | 49.5 | 4 | - | [39] |
| Ni$_{foam}$/Co(OH)$_x$ | 110 | A$_G$ = 2.0<br>*A$_{ECSA}$ = 2813 | | 86.7 | 87.5 | 20 | 6 cycles | |
| Ni$_{foam}$/Cu$_2$O/Co(OH)$_x$ | 110 | A$_G$ = 2.0<br>*A$_{ECSA}$ = 3518 | | 90.3 | 94 | 22 | 6 cycles | |
| Ni$_{foam}$/MnO$_2$-Oxygen vacancy | 110 | A$_G$=8 | | 15.9 | 34.5 | 62.2 | - | |
| Ni$_{foam}$/Pd | 110 | A$_G$=8 | [Na$_2$SO$_4$] = 50 mM [NO$_3^-$] = 1.6 mM<br>$E$ = -0.85 V vs Ag/AgCl<br>Time = 6 h<br>Divided continuous-flow cell | 53.3 | 85 | 69.7 | - | [103] |
| Ni$_{foam}$/MnO$_2$-Oxygen vacancy-Pd | 110 | A$_G$=8 | | 90.6 | 87.6 | 69.6 | - | |
| Ni$_{foam}$/Fe@Fe$_2$O$_3$ | - | *A$_{ECSA}$= 6.5 | [Na$_2$SO$_4$] = 0.1 M [NO$_3^-$] = 3.6 mM<br>$E$ = -1.35 V vs Ag/AgCl | 86.1 | 93 | - | - | [98] |

| Catalyst | | A | Conditions | | | | | Ref. |
|---|---|---|---|---|---|---|---|---|
| Ni$_{foam}$/Co-Fe@Fe$_2$O$_3$ | - | *A$_{ECSA}$= 37.75 | Time = 10 h<br>Undivided cell | 96.7 | 99 | 85.2 | 8 cycles | |
| Ni$_{foam}$/NiCo | - | A$_G$ = 5 | [Na$_2$SO$_4$] = 50 mM [NO$_3^-$] = 3.6 mM<br>$j$ = 2 mA cm$^{-2}$ | 82 | 73.4 | 43.5 | - | [99] |
| Ni$_{foam}$/NiCoP | - | A$_G$ = 5 | Time = 5 h<br>$Q$ = 180 C<br>Divided cell | 97.7 | 95.4 | 57.7 | 6 cycles | |
| Ni$_{foam}$/Co(OH)$_2$ nanowire array | - | A$_G$ = 1.5<br>*A$_{ECSA}$ = 17 | [Na$_2$SO$_4$] = 0.2 M [NO$_3^-$] = 7.14 mM<br>$E$ = -0.7 V vs RHE<br>Time = 3 h<br>Undivided cell | 7.8 | 86.9 | - | - | [100] |
| Ni$_{foam}$/Co$_3$O$_4$ nanowire array | - | A$_G$ = 1.5<br>*A$_{ECSA}$ = 5 | | 13.9 | 88.1 | - | - | |
| Ni$_{foam}$/CoP nanowire array | - | A$_G$ = 1.5<br>*A$_{ECSA}$ = 857 | | 97.9 | 99.4 | 97 | 10 cycles | |
| Ni$_{foam}$/NiCo$_2$O$_4$ | - | A$_G$ = 2<br>A$_{ECSA}$ = 592.5 | [KOH] = 1.0 M [NO$_3^-$] = 3.6 mM<br>$E$ = -1.4 V vs Ag/AgCl | 60.5 | 76.9 | | | [101] |
| Ni$_{foam}$/NiCo$_2$S$_4$ | - | A$_G$ = 2<br>A$_{ECSA}$ = 1006.25 | Time = 2 h<br>Divided cell | 89.6 | 92.1 | 45.4 | 8 cycles | |
| Ni foam | - | A$_G$ = 0.09<br>*A$_{ECSA}$ = 1.0 | [Na$_2$SO$_4$] = 0.1 M [NO$_3^-$] = 500 mM<br>$E$ = -0.9 V vs RHE | - | | 49 | - | [102] |
| Ni$_{foam}$/Ni-BO$_x$ | - | A$_G$ = 0.09<br>*A$_{ECSA}$ = 1.7 | Time = 0.5 h<br>Undivided cell | - | | 94 | 30 cycles | |

578   *ECSA calculated using the specific capacitance 40 µF cm$^{-2}$

579   **ECSA calculated using the specific capacitance 60 µF cm$^{-2}$

580

581 The literature on metal-3D foam electrodes for ERN is extensive, but comparing different

582 electrode materials remains challenging due to the lack of normalization of experimental

583 conditions, reported parameters, and operation methods. Nevertheless, comparing the selected

584 results shown in Tables 3 and 4 allows us to identify five keypoints to be improved in the future.

585 (1) The *PPI* metric is only reported in 30 % of the studies considered. This suggests that

586 either only one value is commonly reported for this parameter or its importance is often

587 overlooked. However, it is crucial to note that various *PPI* values ranging from 5 to 130 are

588 available in the commercially available foams. As previously discussed, *PPI* plays a pivotal role

589 in mass transfer at the electrode surface, making it crucial for controlling the interfacial pH.

590 Therefore, by considering *PPI* as a fixed parameter, the benchmarking process is limited to a very

591 few number of studies.

592 (2) The electrode area, whether geometrical or ECSA, is essential for a comprehensive

593 comparison among the array of electrocatalysts prepared. However, according to the studies

594 considered, geometric 2D area (W x L) is commonly used for reporting performance, overlooking

595 the true effects of 3D structures. Consequently, parameters such as areal density ($cm^2$ $g^{-1}$) or

596 specific surface area (SSA, $cm^2$ $cm^{-3}$) are often neglected. Similarly, ECSA, crucial for intrastudy

597 benchmarking of electrocatalysts and providing insight into modified material and their intrinsic

598 activity (as suggested in Figure 1), is not consistently reported. A more meticulous

599 electrochemical interstudy benchmarking of electrocatalysts requires the estimation of ECSA for

600 a better understanding of the electrochemical system, which is urgently needed. Therefore,

601 reporting both geometric area and ECSA should be promoted as a good practice to enhance the

602 benchmarking of electrocatalysts both within and across studies.

603 (3) Variations in experimental conditions such as initial $NO_3^-$ concentration and

604 electrolyte composition make it difficult to compare different studies, despite most studies

605 providing $NO_3^-$ conversion and $NH_3$ selectivity evaluation. For instance, Cu foam (Table 3, [95])

606 exhibits a $NO_3^-$ conversion of 33.9 % and a $NH_3$ selectivity of 67.1 %, while $Ni_{foam}$/Pd (Table 4,

607 [103]) shows 53.3 % and 85%, respectively. Based solely on conversion values, $Ni_{foam}$/Pd appears

608      to exhibit higher activity, potentially leading to an increased $NH_3$ production. However, such

609      comparisons are inaccurate without considering the initial $NO_3^-$ concentration. Using the reported

610      initial conditions (40 mM $NO_3^-$ for Cu foam and 1.6 mM $NO_3^-$ for $Ni_{foam}$/Pd), Cu foam generates

611      approximately 127 mg $NH_3$-N $L^{-1}$ and $Ni_{foam}$/Pd 10.14 mg $NH_3$-N $L^{-1}$. This highlights the

612      challenge of benchmarking electrodes using these parameters, which involves considering the

613      initial $NO_3^-$ concentration and subsequent calculations to enable direct comparison. Furthermore,

614      the absence of standardized conditions results in a chaotic range of conditions, with initial $NO_3^-$

615      concentrations varying from 1 to 40 mM for Cu-based electrodes (Table 3) and from 2 to 500 mM

616      for Ni-based electrodes (Table 4).

617          (4) Similarly to the wide range of initial $NO_3^-$ concentrations, electrochemical conditions

618      are not standardized across studies. Under potentiostatic conditions, reported potentials in

619      electrolysis correspond to those determined during the evaluation of intrinsic activity. However,

620      key parameters such as supporting electrolytes, initial pH, and electrolysis time are often different.

621      A subset of studies performs electrolysis under galvanostatic conditions, employing current

622      densities ranging from 2 to 40 mA $cm^{-2}$, but without considering a benchmark and constant

623      number of coulombs circulated during the electrolysis to facilitate subsequent results comparison.

624      Notably, comparing results from Tables 3 and 4 reveals some trends; for example, disparities in

625      $FE_{NH3}$ arise when comparing constant potential electrolysis (mostly $FE_{NH3} \geq 70\%$) with constant

626      current electrolysis (mostly $FE_{NH3} < 30\%$). The main reason for these disparities lies in the

627      competitive hydrogen evolution reaction (HER), which occurs at a similar potential to ERN. HER

628      can be modulated by controlling the applied potential, whereas this control is absent in constant

629      current electrolysis. Consequently, the quantification of $H_2$ gas produced during ERN electrolysis

630      represents a significant gap in most ERN studies, which is typically overlooked. Comparison

631      across operation methods is incorrect as it will not illustrate the competitiveness of

632      electrocatalysts under identical conditions. Furthermore, the reader should note that real upscale

633      applications generally operate under galvanostatic conditions in large electrochemically

engineered systems beyond the lab bench (which would correspond to the studies that report the lower $FE_{NH_3}$ values in literature).

(5) The most commonly used benchmarking parameter for ERN in the literature, $NH_3$ yield (mmol $NH_3$ $g^{-1}_{cat}$ $h^{-1}$ or mmol $NH_3$ $cm^{-2}_{cat}$ $h^{-1}$), directly incorporates $NH_3$ production normalized by catalyst mass or area, and time. However, the disparities between geometrical and ECSA areas introduce additional errors in reporting $NH_3$ yield. This parameter introduces another source of confusion since at high initial $NO_3^-$ concentrations, $NH_3$ yield produced on a poor electrocatalyst may appear higher than that obtained using an optimal electrode, but treating a lower initial $NO_3^-$ concentration. Therefore, there is an urgent need to incorporate additional parameters, which consider the initial $NO_3^-$ concentration to avoid misunderstandings and facilitate benchmarking, as well as evaluate the overpotential and, thus, the energy required to produce $NH_3$. We have recently proposed $NH_3$ generation efficiency (Equation (10)) [90], which combines both concepts, selectivity and conversion.

$$NH_3 \ generation \ efficiency \ (\%) = \frac{C_{NH_3,exp}}{C_{NH_3,theo}} \times 100 \tag{10}$$

where $C_{NH_3,exp}$ is the $NH_3$ concentration experimentally obtained from electrolysis in mmol $L^{-1}$ and $C_{NH_3,theo}$ is the theoretical $NH_3$ concentration in mmol $L^{-1}$ if the entire initial amount of $NO_3^-$ is converted to $NH_3$ by ERN.

Concerning the overpotential evaluation in $NO_3^-$ conversion, we propose to adapt the parameter of energy efficiency (Equation (11)), which is commonly used to evaluate electrochemical $CO_2$ reduction performance [104,105].

$$NH_3 \ energy \ efficiency \ (\%) = (E_T/E) \ x \ FE_{NH_3} \tag{11}$$

where $E_T$ is the thermodynamic potential in volts required for the electrocatalytic reduction of $NO_3^-$ to $NH_3$ in aqueous solution, whereas $E$ and $FE_{NH_3}$ represent the experimental cathode potential applied in volts and the $NH_3$ Faradaic Efficiency (%), respectively.

## 4. Conclusions and outlook

The ERN systems have emerged as a promising approach for resource recovery, particularly in $NH_3$ production. Rational electrode design has guided researchers through various configurations, with metal-based 3D electrodes showing considerable potential in material design. Specifically, self-standing Cu and Ni foam electrodes have been extensively studied for their roles as electrocatalytic active and support materials, respectively. This review addresses two critical parameters characterizing foam electrodes often overlooked in ERN literature: pore per inch (*PPI*) and electrochemically active surface area (ECSA), as well as proposes two additional engineering figures of merit for benchmarking ERN by encompassing selectivity and conversion and evaluating overpotential contribution.

The importance of *PPI* is revalued, emphasizing its significant role in reactants and products mass transfer, and suggesting its crucial relevance in evaluating water matrices to prevent inorganic and organic scaling. However, the lack of studies using full reactors (flow-through or flow-by) conceals the benefits of 3D metal foam for ERN. Additionally, the indirect measurement of ECSA is promoted, with main steps provided for reliable calculations. Techniques such as cyclic voltammetry or electrochemical impedance spectroscopy can be utilized to estimate ECSA, with consistency across studies recommended for proper evaluation of modified Cu and Ni foam electrodes ($Cu_{foam}$/M and $Ni_{foam}$/M).

At present, benchmarking electrocatalysts for ERN presents more challenges than certainties. Despite ERN's potential as a resource recovery approach, the lack of specific trends and variety among studies creates a complex scenario where comparability is limited. Significant advances have been made in electrocatalyst design, but some reference values have not been identified yet. The current lack of standardization in reporting *PPI*, ECSA, experimental conditions, and key performance metrics hinders meaningful comparisons across ERN studies. This variability limits a broader understanding of the ERN and obscures the identification of optimal electrode materials and operating parameters. Reviewing $Cu_{foam}$/M and $Ni_{foam}$/M studies reveals nuances based on various aspects, prompting reconsideration of the composition of the solution to be treated and

the need to set reference concentrations for both reactant and supporting electrolyte, as well as using a constant amount of circulated charge to compare different electrolysis properly. Morphological and structural analysis of the electrode before and after ERN electrolysis is notably absent in the literature. Similarly, accelerated life tests for these 3D foam electrodes are rarely considered.

From this perspective, several key research directions are essential and require future development. Reactor configurations designed to optimize 3D foam electrodes and strategies to suppress the competitive HER could significantly improve ERN efficiency. Exploring electrocatalytic materials that selectively inhibit HER without impacting ERN could be a promising research direction, particularly relevant in galvanostatic electrolysis. Additionally, investigations in electrode stability under realistic water conditions by accelerated tests, considering potential issues like inorganic scaling, are crucial for practical applications.

The benchmarking of 3D electrodes for ERN represents a significant challenge, as highlighted by the nuances and gaps identified in this review. It is evident that the current state of research lacks characterization protocols and standardized reporting practices, which hinders effective comparison of electrode performance across studies. By addressing these challenges, we should be able to accelerate the development of highly efficient, selective, and scalable ERN systems, propelling this technology, still under development, from a low technology readiness level (TRL) towards a widespread water treatment technology. While significant advances have been made in understanding the fundamental principles of ERN and exploring novel electrodes configurations, there remains a need for practical implementation and field testing under real-world conditions.

**Acknowledgements**

718

## 5. References

[1] A.J. dos Santos, H.L. Barazorda-Ccahuana, G. Caballero-Manrique, Y. Chérémond, P.J. Espinoza-Montero, J.R. González-Rodríguez, U.J. Jáuregui-Haza, M.R.V. Lanza, A. Nájera, C. Oporto, A. Pérez Parada, T. Pérez, V.D. Quezada, V. Rojas, V. Sosa, A. Thiam, R.A. Torres-Palma, R. Vargas, S. Garcia-Segura, Accelerating innovative water treatment in Latin America, Nat. Sustain. (2023). https://doi.org/10.1038/s41893-022-01042-z.

[2] I. Jeon, E.C. Ryberg, P.J.J. Alvarez, J.H. Kim, Technology assessment of solar disinfection for drinking water treatment, Nat. Sustain. 5 (2022). https://doi.org/10.1038/s41893-022-00915-7.

[3] N. Singh, B.R. Goldsmith, Role of Electrocatalysis in the Remediation of Water Pollutants, ACS Catal. 10 (2020) 3365–3371. https://doi.org/10.1021/acscatal.9b04167.

[4] I. Katsounaros, On the assessment of electrocatalysts for nitrate reduction, Curr. Opin. Electrochem. 28 (2021) 100721. https://doi.org/10.1016/j.coelec.2021.100721.

[5] D. Cecconet, F. Sabba, M. Devecseri, A. Callegari, A.G. Capodaglio, In situ groundwater remediation with bioelectrochemical systems: A critical review and future perspectives, Environ. Int. 137 (2020) 105550. https://doi.org/10.1016/j.envint.2020.105550.

[6] M.J. Pennino, J.E. Compton, S.G. Leibowitz, Trends in Drinking Water Nitrate Violations Across the United States, Environ. Sci. Technol. 51 (2017) 13450–13460. https://doi.org/10.1021/acs.est.7b04269.

[7] M. Allaire, H. Wu, U. Lall, National trends in drinking water quality violations, Proc. Natl. Acad. Sci. U. S. A. 115 (2018) 2078–2083. https://doi.org/10.1073/pnas.1719805115.

[8] M. Allaire, H. Wu, U. Lall, National trends in drinking water quality violations, Proc.

744          Natl. Acad. Sci. U. S. A. 115 (2018) 2078–2083.

745          https://doi.org/10.1073/pnas.1719805115.

746    [9]    R. Epsztein, O. Nir, O. Lahav, M. Green, Selective nitrate removal from groundwater

747          using a hybrid nanofiltration-reverse osmosis filtration scheme, Chem. Eng. J. 279

748          (2015) 372–378. https://doi.org/10.1016/j.cej.2015.05.010.

749    [10]    A.M. Bergquist, J.K. Choe, T.J. Strathmann, C.J. Werth, Evaluation of a hybrid ion

750          exchange-catalyst treatment technology for nitrate removal from drinking water, Water

751          Res. 96 (2016) 177–187. https://doi.org/10.1016/j.watres.2016.03.054.

752    [11]    S. Singh, A.G. Anil, V. Kumar, D. Kapoor, S. Subramanian, J. Singh, P.C. Ramamurthy,

753          Nitrates in the environment: A critical review of their distribution, sensing techniques,

754          ecological effects and remediation, Chemosphere. 287 (2022) 131996.

755          https://doi.org/10.1016/j.chemosphere.2021.131996.

756    [12]    B.K. Pramanik, L. Shu, V. Jegatheesan, A review of the management and treatment of

757          brine solutions, Environ. Sci. Water Res. Technol. 3 (2017) 625–658.

758          https://doi.org/10.1039/c6ew00339g.

759    [13]    J. Sanchis-Carbonell, I. Carrero-Ferrer, A. Sáez-Fernández, M. Pedro-Monzonís, P.

760          Campíns-Falcó, V. Montiel, Towards a zero liquid discharge process from brine

761          treatment: Water recovery, nitrate electrochemical elimination and potential valorization

762          of hydrogen and salts, Sci. Total Environ. 926 (2024).

763          https://doi.org/10.1016/j.scitotenv.2024.172060.

764    [14]    S. Garcia-Segura, M. Lanzarini-Lopes, K. Hristovski, P. Westerhoff, Electrocatalytic

765          reduction of nitrate: Fundamentals to full-scale water treatment applications, Appl. Catal.

766          B Environ. 236 (2018) 546–568. https://doi.org/10.1016/j.apcatb.2018.05.041.

767    [15]    K. Flores, G.A. Cerrón-Calle, C. Valdes, A. Atrashkevich, A. Castillo, H. Morales, J.G.

768          Parsons, S. Garcia-Segura, J.L. Gardea-Torresdey, Outlining Key Perspectives for the

769        Advancement of Electrocatalytic Remediation of Nitrate from Polluted Waters, ACS

770        ES&T Eng. 2 (2022) 746–768. https://doi.org/10.1021/acsestengg.2c00052.

771   [16]  M. Marcos-Hernández, G. Antonio Cerrón-Calle, Y. Ge, S. Garcia-Segura, C.M.

772        Sánchez-Sánchez, A.S. Fajardo, D. Villagrán, Effect of surface functionalization of

773        Fe3O4 nano-enabled electrodes on the electrochemical reduction of nitrate, Sep. Purif.

774        Technol. 282 (2022) 119771. https://doi.org/10.1016/j.seppur.2021.119771.

775   [17]  G.A. Cerrón-Calle, A.S. Fajardo, J. Liu, C.M. Sánchez-Sánchez, S. Garcia-Segura,

776        Enabling circular economy by N-recovery: Electrocatalytic reduction of nitrate with

777        cobalt hydroxide nanocomposites on copper foam treating low conductivity groundwater

778        effluents, Sci. Total Environ. 887 (2023) 163938.

779        https://doi.org/10.1016/j.scitotenv.2023.163938.

780   [18]  D. Anastasiadou, Y. van Beek, W. Chen, T. Wissink, A. Parastaev, E.J.M. Hensen, M.

781        Costa Figueiredo, Morphology Changes of Cu2O Catalysts During Nitrate

782        Electroreduction to Ammonia**, ChemCatChem. 15 (2023) 1–9.

783        https://doi.org/10.1002/cctc.202201503.

784   [19]  A.S. Fajardo, P. Westerhoff, S. Garcia-Segura, C.M. Sánchez-Sánchez, Selectivity

785        modulation during electrochemical reduction of nitrate by electrolyte engineering, Sep.

786        Purif. Technol. 321 (2023) 124233. https://doi.org/10.1016/j.seppur.2023.124233.

787   [20]  J.M. McEnaney, S.J. Blair, A.C. Nielander, J.A. Schwalbe, D.M. Koshy, M. Cargnello,

788        T.F. Jaramillo, Electrolyte engineering for efficient electrochemical nitrate reduction to

789        ammonia on a titanium electrode, ACS Sustain. Chem. Eng. 8 (2020) 2672–2681.

790        https://doi.org/10.1021/acssuschemeng.9b05983.

791   [21]  I. Sanjuán, L. García-Cruz, J. Solla-Gullón, E. Expósito, V. Montiel, Bi–Sn

792        nanoparticles for electrochemical denitrification: activity and selectivity towards N2

793        formation, Electrochim. Acta. 340 (2020).

794        https://doi.org/10.1016/j.electacta.2020.135914.

795   [22]   D.R. MacFarlane, P. V. Cherepanov, J. Choi, B.H.R. Suryanto, R.Y. Hodgetts, J.M.

796            Bakker, F.M. Ferrero Vallana, A.N. Simonov, A Roadmap to the Ammonia Economy,

797            Joule. 4 (2020) 1186–1205. https://doi.org/10.1016/j.joule.2020.04.004.

798   [23]   P.H. van Langevelde, I. Katsounaros, M.T.M. Koper, Electrocatalytic Nitrate Reduction

799            for Sustainable Ammonia Production, Joule. 5 (2021) 290–294.

800            https://doi.org/10.1016/j.joule.2020.12.025.

801   [24]   H. Yin, X. Xing, W. Zhang, J. Li, W. Xiong, H. Li, A simple hydrothermal synthesis of

802            an oxygen vacancy-rich MnMoO4 rod-like material and its highly efficient

803            electrocatalytic nitrogen reduction, Dalt. Trans. 52 (2023) 16670–16679.

804            https://doi.org/10.1039/d3dt03018k.

805   [25]   X. Huang, X. Xing, W. Xiong, H. Li, Flower-Like Ni-Mn Bimetallic Oxide-Based

806            Nanosheets for Enhanced Electrocatalytic Nitrogen Reduction to Ammonia, Energy and

807            Fuels. 37 (2023) 19147–19155. https://doi.org/10.1021/acs.energyfuels.3c03517.

808   [26]   G.A. Cerrón-Calle, T.P. Senftle, S. Garcia-Segura, Strategic tailored design of

809            electrocatalysts for environmental remediation based on density functional theory (DFT)

810            and microkinetic modeling, Curr. Opin. Electrochem. 35 (2022) 101062.

811            https://doi.org/10.1016/j.coelec.2022.101062.

812   [27]   Y. Wang, W. Zhou, R. Jia, Y. Yu, B. Zhang, Unveiling the Activity Origin of a Copper-

813            based Electrocatalyst for Selective Nitrate Reduction to Ammonia, Angew. Chemie - Int.

814            Ed. 59 (2020) 5350–5354. https://doi.org/10.1002/anie.201915992.

815   [28]   D. Hao, Z. gang Chen, M. Figiela, I. Stepniak, W. Wei, B.J. Ni, Emerging alternative for

816            artificial ammonia synthesis through catalytic nitrate reduction, J. Mater. Sci. Technol.

817            77 (2021) 163–168. https://doi.org/10.1016/j.jmst.2020.10.056.

818   [29]   L. Yang, J. Li, F. Du, J. Gao, H. Liu, S. Huang, H. Zhang, C. Li, C. Guo, Interface

819            engineering cerium-doped copper nanocrystal for efficient electrochemical nitrate-to-

820      ammonia production, Electrochim. Acta. 411 (2022) 140095.

821      https://doi.org/10.1016/j.electacta.2022.140095.

822   [30]  Z. Niu, S. Fan, X. Li, J. Duan, A. Chen, Interfacial engineering of CoMn2O4/NC

823      induced electronic delocalization boosts electrocatalytic nitrogen oxyanions reduction to

824      ammonia, Appl. Catal. B Environ. 322 (2023) 122090.

825      https://doi.org/10.1016/j.apcatb.2022.122090.

826   [31]  A. Atrashkevich, A.S. Fajardo, P. Westerhoff, W.S. Walker, C.M. Sánchez-Sánchez, S.

827      Garcia-Segura, Overcoming barriers for nitrate electrochemical reduction: By-passing

828      water hardness, Water Res. 225 (2022) 119118.

829      https://doi.org/10.1016/j.watres.2022.119118.

830   [32]  J. Ma, W. Wei, G. Qin, T. Xiao, W. Tang, S. Zhao, L. Jiang, S. Liu, Electrochemical

831      reduction of nitrate in a catalytic carbon membrane nano-reactor, Water Res. 208 (2022)

832      117862. https://doi.org/10.1016/j.watres.2021.117862.

833   [33]  J. Li, G. Zhan, J. Yang, F. Quan, C. Mao, Y. Liu, B. Wang, F. Lei, L. Li, A.W.M. Chan,

834      L. Xu, Y. Shi, Y. Du, W. Hao, P.K. Wong, J. Wang, S.X. Dou, L. Zhang, J.C. Yu,

835      Efficient Ammonia Electrosynthesis from Nitrate on Strained Ruthenium Nanoclusters,

836      J. Am. Chem. Soc. 142 (2020) 7036–7046. https://doi.org/10.1021/jacs.0c00418.

837   [34]  A. Iarchuk, A. Dutta, P. Broekmann, Novel Ni foam catalysts for sustainable nitrate to

838      ammonia electroreduction, J. Hazard. Mater. 439 (2022) 129504.

839      https://doi.org/10.1016/j.jhazmat.2022.129504.

840   [35]  A. Kulshreshtha, S.K. Dhakad, Preparation of metal foam by different methods: A

841      review, Mater. Today Proc. 26 (2019) 1784–1790.

842      https://doi.org/10.1016/j.matpr.2020.02.375.

843   [36]  M. Grdeń, M. Alsabet, G. Jerkiewicz, Surface science and electrochemical analysis of

844      nickel foams, ACS Appl. Mater. Interfaces. 4 (2012) 3012–3021.

845      https://doi.org/10.1021/am300380m.

846    [37]   A.S. Fajardo, P. Westerhoff, C.M. Sanchez-Sanchez, S. Garcia-Segura, Earth-abundant

847           elements a sustainable solution for electrocatalytic reduction of nitrate, Appl. Catal. B

848           Environ. 281 (2021) 119465. https://doi.org/10.1016/j.apcatb.2020.119465.

849    [38]   G.A. Cerrón-Calle, A.S. Fajardo, C.M. Sánchez-Sánchez, S. Garcia-Segura, Highly

850           reactive Cu-Pt bimetallic 3D-electrocatalyst for selective nitrate reduction to ammonia,

851           Appl. Catal. B Environ. 302 (2022) 120844.

852           https://doi.org/10.1016/j.apcatb.2021.120844.

853    [39]   G.A. Cerrón-Calle, A. Wines, S. Garcia-Segura, Atomic hydrogen provision by cobalt

854           sites in a bimetallic Ni/Co(OH)x and trimetallic Ni/Cu2O/Co(OH)x configurations for

855           superior ammonia production, Appl. Catal. B Environ. 328 (2023) 122540.

856           https://doi.org/10.1016/j.apcatb.2023.122540.

857    [40]   C.C.L. McCrory, S. Jung, J.C. Peters, T.F. Jaramillo, Benchmarking heterogeneous

858           electrocatalysts for the oxygen evolution reaction, J. Am. Chem. Soc. 135 (2013) 16977–

859           16987. https://doi.org/10.1021/ja407115p.

860    [41]   Y. Guan, W. Suo, Z. Zhang, Y. Wang, S. Sun, G. Liu, Insights on the Catalytic Active

861           Site for CO2 Reduction on Copper-based Catalyst: A DFT study, Mol. Catal. 511 (2021)

862           111725. https://doi.org/10.1016/j.mcat.2021.111725.

863    [42]   N. Atrak, E. Tayyebi, E. Skúlason, Effect of co-adsorbed water on electrochemical CO2

864           reduction reaction on transition metal oxide catalysts, Appl. Surf. Sci. 570 (2021)

865           151031. https://doi.org/10.1016/j.apsusc.2021.151031.

866    [43]   D. Jang, J. Maeng, J. Kim, H. Han, G.H. Park, J. Ha, D. Shin, Y.J. Hwang, W.B. Kim,

867           Boosting electrocatalytic nitrate reduction reaction for ammonia synthesis by plasma-

868           induced oxygen vacancies over MnCuOx, Appl. Surf. Sci. 610 (2023) 155521.

869           https://doi.org/10.1016/j.apsusc.2022.155521.

870     [44]    W. Zheng, Y. Chen, X. Peng, K. Zhong, Y. Lin, Z. Huang, The phase evolution and

871           physical properties of binary copper oxide thin films prepared by reactive magnetron

872           sputtering, Materials (Basel). 10 (2018) 1–13. https://doi.org/10.3390/ma11071253.

873     [45]    M.I. Pintor-Monroy, D. Barrera, B.L. Murillo-Borjas, F.J. Ochoa-Estrella, J.W.P. Hsu,

874           M.A. Quevedo-Lopez, Tunable Electrical and Optical Properties of Nickel Oxide (NiO x

875           ) Thin Films for Fully Transparent NiO x -Ga 2 O 3 p-n Junction Diodes, ACS Appl.

876           Mater. Interfaces. 10 (2018) 38159–38165. https://doi.org/10.1021/acsami.8b08095.

877     [46]    N.D. Koshel', V. V. Malyshev, Measurement of the resistivity of the electrode

878           NiOOH/Ni(OH)2 solid phase active substance during the discharge process, Surf. Eng.

879           Appl. Electrochem. 46 (2010) 348–351. https://doi.org/10.3103/S1068375510040095.

880     [47]    H. Bartzsch, D. Glöß, B. Böcher, P. Frach, K. Goedicke, Properties of SiO2 and Al2O3

881           films for electrical insulation applications deposited by reactive pulse magnetron

882           sputtering, Surf. Coatings Technol. 174–175 (2003) 774–778.

883           https://doi.org/10.1016/S0257-8972(03)00384-0.

884     [48]    J. Liu, J. Dang, M. Wang, X. Wang, X. Duan, S. Yuan, T. Liu, Q. Wang, Metal–

885           Organic-Framework-Derived Cobalt nanoparticles encapsulated in Nitrogen-Doped

886           carbon nanotubes on Ni foam integrated Electrode: Highly electroactive and durable

887           catalysts for overall water splitting, J. Colloid Interface Sci. 606 (2022) 38–46.

888           https://doi.org/10.1016/j.jcis.2021.07.152.

889     [49]    W. Wu, J. Liu, N. Johannes, Electrodeposition of Ir–Co thin films on copper foam as

890           high-performance electrocatalysts for efficient water splitting in alkaline medium, Int. J.

891           Hydrogen Energy. 46 (2021) 609–621. https://doi.org/10.1016/j.ijhydene.2020.09.268.

892     [50]    N. Girichandran, S. Saedy, R. Kortlever, Electrochemical CO2 reduction on a copper

893           foam electrode at elevated pressures, Chem. Eng. J. 487 (2024) 150478.

894           https://doi.org/10.1016/j.cej.2024.150478.

895 [51] W. Zheng, M. Liu, L.Y.S. Lee, Best Practices in Using Foam-Type Electrodes for

896 Electrocatalytic Performance Benchmark, ACS Energy Lett. 5 (2020) 3260–3264.

897 https://doi.org/10.1021/acsenergylett.0c01958.

898 [52] J. Van Drunen, B. Kinkead, M.C.P. Wang, E. Sourty, B.D. Gates, G. Jerkiewicz,

899 Comprehensive structural, surface-chemical and electrochemical characterization of

900 nickel-based metallic foams, ACS Appl. Mater. Interfaces. 5 (2013) 6712–6722.

901 https://doi.org/10.1021/am401606n.

902 [53] Y.J. Shih, Z.L. Wu, Y.H. Huang, C.P. Huang, Electrochemical nitrate reduction as

903 affected by the crystal morphology and facet of copper nanoparticles supported on nickel

904 foam electrodes (Cu/Ni), Chem. Eng. J. 383 (2020) 123157.

905 https://doi.org/10.1016/j.cej.2019.123157.

906 [54] F. Jamshidi, W. Kunz, P. Altschuh, T. Lu, M. Laqua, A. August, F. Löffler, M. Selzer,

907 B. Nestler, A 3D computational method for determination of pores per inch (PPI) of

908 porous structures, Mater. Today Commun. 34 (2023) 105413.

909 https://doi.org/10.1016/j.mtcomm.2023.105413.

910 [55] S. Das, N.G. Deen, J.A.M. Kuipers, Multiscale modeling of fixed-bed reactors with

911 porous (open-cell foam) non-spherical particles: Hydrodynamics, Chem. Eng. J. 334

912 (2018) 741–759. https://doi.org/10.1016/j.cej.2017.10.047.

913 [56] I. Mohammed, T. Bauer, M. Schubert, R. Lange, Hydrodynamic multiplicity in a tubular

914 reactor with solid foam packings, Chem. Eng. J. 231 (2013) 334–344.

915 https://doi.org/10.1016/j.cej.2013.07.024.

916 [57] L.F. Arenas, C. Ponce de León, F.C. Walsh, 3D-printed porous electrodes for advanced

917 electrochemical flow reactors: A Ni/stainless steel electrode and its mass transport

918 characteristics, Electrochem. Commun. 77 (2017) 133–137.

919 https://doi.org/10.1016/j.elecom.2017.03.009.

920 [58] A.S. Suleiman, N. Dukhan, Long-domain simulation of flow in open-cell mesoporous

921 metal foam and direct comparison to experiment, Microporous Mesoporous Mater. 196

922 (2014) 104–114. https://doi.org/10.1016/j.micromeso.2014.05.003.

923 [59] F.J. Recio, P. Herrasti, L. Vazquez, C. Ponce De León, F.C. Walsh, Mass transfer to a

924 nanostructured nickel electrodeposit of high surface area in a rectangular flow channel,

925 Electrochim. Acta. 90 (2013) 507–513. https://doi.org/10.1016/j.electacta.2012.11.135.

926 [60] D.F.S. Morais, J.C.B. Lopes, M.M. Dias, V.J.P. Vilar, F.C. Moreira, e–NETmix: A

927 pioneering electrochemical flow reactor with enhanced mass transfer, Chem. Eng. J. 481

928 (2024). https://doi.org/10.1016/j.cej.2023.148244.

929 [61] Z. Qiao, Z. Wang, C. Zhang, S. Yuan, Y. Zhu, J. Wang, PVAm–PIP/PS composite

930 membrane with high performance for $CO_2/N_2$ separation, AIChE J. 59 (2012) 215–228.

931 https://doi.org/10.1002/aic.

932 [62] W.S. Walker, E. Bezerra Cavalcanti, A. Atrashkevich, A.S. Fajardo, E. Brillas, S.

933 Garcia-Segura, Mass transfer and residence time distribution in an electrochemical cell

934 with an air-diffusion electrode: Effect of air pressure and mesh promoters, Electrochim.

935 Acta. 378 (2021) 138131. https://doi.org/10.1016/j.electacta.2021.138131.

936 [63] M.J. Kim, Y. Seo, M.A. Cruz, B.J. Wiley, Metal Nanowire Felt as a Flow-Through

937 Electrode for High-Productivity Electrochemistry, ACS Nano. 13 (2019) 6998–7009.

938 https://doi.org/10.1021/acsnano.9b02058.

939 [64] Y. Chen, G. Zhang, Q. Ji, H. Lan, H. Liu, J. Qu, Visualization of Electrochemically

940 Accessible Sites in Flow-through Mode for Maximizing Available Active Area toward

941 Superior Electrocatalytic Ammonia Oxidation, Environ. Sci. Technol. 56 (2022) 9722–

942 9731. https://doi.org/10.1021/acs.est.2c01707.

943 [65] M.C.O. Monteiro, A. Mirabal, L. Jacobse, K. Doblhoff-Dier, S.C. Barton, M.T.M.

944 Koper, Time-Resolved Local pH Measurements during CO2Reduction Using Scanning

945       Electrochemical Microscopy: Buffering and Tip Effects, JACS Au. 1 (2021) 1915–1924.

946       https://doi.org/10.1021/jacsau.1c00289.

947  [66]  M.C.O. Monteiro, M.T.M. Koper, Measuring local pH in electrochemistry, Curr. Opin.

948       Electrochem. 25 (2021) 100649. https://doi.org/10.1016/j.coelec.2020.100649.

949  [67]  J.H. Han, Exploring the Interface of Porous Cathode/Bipolar Membrane for Mitigation

950       of Inorganic Precipitates in Direct Seawater Electrolysis, ChemSusChem. 15 (2022).

951       https://doi.org/10.1002/cssc.202200372.

952  [68]  R. Mao, H. Zhu, K.F. Wang, X. Zhao, Selective conversion of nitrate to nitrogen gas by

953       enhanced electrochemical process assisted by reductive Fe(II)-Fe(III) hydroxides at

954       cathode surface, Appl. Catal. B Environ. 298 (2021) 120552.

955       https://doi.org/10.1016/j.apcatb.2021.120552.

956  [69]  M.D. Patil, S.D. Dhas, A.A. Mane, A. V. Moholkar, Clinker-like V2O5 nanostructures

957       anchored on 3D Ni-foam for supercapacitor application, Mater. Sci. Semicond. Process.

958       133 (2021) 105978. https://doi.org/10.1016/j.mssp.2021.105978.

959  [70]  M. Thommes, K. Kaneko, A. V. Neimark, J.P. Olivier, F. Rodriguez-Reinoso, J.

960       Rouquerol, K.S.W. Sing, Physisorption of gases, with special reference to the evaluation

961       of surface area and pore size distribution (IUPAC Technical Report), Pure Appl. Chem.

962       87 (2015) 1051–1069. https://doi.org/10.1515/pac-2014-1117.

963  [71]  E. Gregorová, T. Uhlířová, W. Pabst, P. Diblíková, I. Sedlářová, Microstructure

964       characterization of mullite foam by image analysis, mercury porosimetry and X-ray

965       computed microtomography, Ceram. Int. 44 (2018) 12315–12328.

966       https://doi.org/10.1016/j.ceramint.2018.04.019.

967  [72]  S. Trasatti, O.A. Petrii, International Union of Pure and Applied Chemistry Physical

968       Chemistry Division Commission on Electrochemistry: Real Surface Area Measurements

969       in Electrochemistry, Pure Appl. Chem. 63 (1991) 711–734.

970        https://doi.org/10.1351/pac199163050711.

971    [73]   A. Lasia, A. Rami, Kinetics of hydrogen evolution on nickel electrodes, J. Electroanal.

972        Chem. 294 (1990) 123–141. https://doi.org/10.1016/0022-0728(90)87140-F.

973    [74]   T.R.L.C. Paixão, Measuring Electrochemical Surface Area of Nanomaterials versus the

974        Randles−Ševčík Equation, ChemElectroChem. 7 (2020) 3414–3415.

975        https://doi.org/10.1002/celc.202000633.

976    [75]   P. Connor, J. Schuch, B. Kaiser, W. Jaegermann, The Determination of Electrochemical

977        Active Surface Area and Specific Capacity Revisited for the System MnOx as an

978        Oxygen Evolution Catalyst, Zeitschrift Fur Phys. Chemie. 234 (2020) 979–994.

979        https://doi.org/10.1515/zpch-2019-1514.

980    [76]   C. Hurth, C. Li, A.J. Bard, Direct probing of electrical double layers by scanning

981        electrochemical potential microscopy, J. Phys. Chem. C. 111 (2007) 4620–4627.

982        https://doi.org/10.1021/jp0661084.

983    [77]   A.J. Bard, L.R. Faulkner, Fundamentals and Applications Plasmonics : Fundamentals

984        and Applications, 2nd ed., John Wiley & Sons, Inc., 2001.

985    [78]   O. Gharbi, M.T.T. Tran, M.E. Orazem, B. Tribollet, M. Turmine, V. Vivier, Impedance

986        Response of a Thin Film on an Electrode: Deciphering the Influence of the Double Layer

987        Capacitance, ChemPhysChem. 22 (2021) 1371–1378.

988        https://doi.org/10.1002/cphc.202100177.

989    [79]   D.M. Morales, M. Risch, Seven steps to reliable cyclic voltammetry measurements for

990        the determination of double layer capacitance, JPhys Energy. 3 (2021) 034013.

991        https://doi.org/10.1088/2515-7655/abee33.

992    [80]   S. Akkari, V. Vivier, C.M. Sánchez-Sánchez, Urea electro-oxidation byproducts impact

993        on NiO/NiOOH anode performance studied by operando electrochemical impedance

994        spectroscopy, Electrochim. Acta. 474 (2024) 143526.

995       https://doi.org/10.1016/j.electacta.2023.143526.

996    [81]    G.J. Brug, A.L.G. van den Eeden, M. Sluyters-Rehbach, J.H. Sluyters, The analysis of

997       electrode impedances complicated by the presence of a constant phase element, J.

998       Electroanal. Chem. 176 (1984) 275–295. https://doi.org/10.1016/S0022-0728(84)80324-

999       1.

1000   [82]    O. Gharbi, M.T.T. Tran, B. Tribollet, M. Turmine, V. Vivier, Revisiting cyclic

1001       voltammetry and electrochemical impedance spectroscopy analysis for capacitance

1002       measurements, Electrochim. Acta. 343 (2020) 136109.

1003       https://doi.org/10.1016/j.electacta.2020.136109.

1004   [83]    S.P. Zankowski, P.M. Vereecken, Electrochemical Determination of Porosity and

1005       Surface Area of Thin Films of Interconnected Nickel Nanowires, J. Electrochem. Soc.

1006       166 (2019) D227–D235. https://doi.org/10.1149/2.0311906jes.

1007   [84]    U.S.G. Survey, Rare Earth Elements — Critical Resources for High Technology, (2002)

1008       1–11.

1009   [85]    X. Lu, H. Song, J. Cai, S. Lu, Recent development of electrochemical nitrate reduction

1010       to ammonia: A mini review, Electrochem. Commun. 129 (2021) 107094.

1011       https://doi.org/10.1016/j.elecom.2021.107094.

1012   [86]    J. Gao, B. Jiang, C. Ni, Y. Qi, X. Bi, Enhanced reduction of nitrate by noble metal-free

1013       electrocatalysis on P doped three-dimensional Co3O4 cathode: Mechanism exploration

1014       from both experimental and DFT studies, Chem. Eng. J. 382 (2020) 123034.

1015       https://doi.org/10.1016/j.cej.2019.123034.

1016   [87]    Y. Wang, C. Wang, M. Li, Y. Yu, B. Zhang, Nitrate electroreduction: Mechanism

1017       insight,: In situ characterization, performance evaluation, and challenges, Chem. Soc.

1018       Rev. 50 (2021) 6720–6733. https://doi.org/10.1039/d1cs00116g.

1019   [88]    X. bo Li, G. ri Xu, Hydrothermal vs electrodeposition: How does deposition method

affect the electrochemical capacitor performance of manganese dioxide?, Ceram. Int. 43 (2017) 8963–8969. https://doi.org/10.1016/j.ceramint.2017.04.036.

[89] D. Taherinia, M. Moazzeni, S. Moravej, Comparison of hydrothermal and electrodeposition methods for the synthesis of CoSe2/CeO2 nanocomposites as electrocatalysts toward oxygen evolution reaction, Int. J. Hydrogen Energy. 47 (2022) 17650–17661. https://doi.org/10.1016/j.ijhydene.2022.03.257.

[90] G.A. Cerrón-Calle, A. Maya, D. Leon, M. Roldan, A.S. Fajardo, C.M. Sánchez-Sánchez, S. Garcia-Segura, Unlocking Sustainable Nitrate Reduction: Earth-Abundant Bimetallic Electrodes Under Galvanostatic Evaluation, Electrochim. Acta. (2024) 144263. https://doi.org/10.1016/j.electacta.2024.144263.

[91] Y. Xu, Y. Sheng, M. Wang, T. Ren, K. Shi, Z. Wang, X. Li, L. Wang, H. Wang, Interface coupling induced built-in electric fields boost electrochemical nitrate reduction to ammonia over CuO@MnO2 core-shell hierarchical nanoarrays, J. Mater. Chem. A. 10 (2022) 16883–16890. https://doi.org/10.1039/d2ta02006h.

[92] C. Zhou, J. Bai, Y. Zhang, J. Li, Z. Li, P. Jiang, F. Fang, M. Zhou, X. Mei, B. Zhou, Novel 3D Pd-Cu(OH)2/CF cathode for rapid reduction of nitrate-N and simultaneous total nitrogen removal from wastewater, J. Hazard. Mater. 401 (2021) 123232. https://doi.org/10.1016/j.jhazmat.2020.123232.

[93] X. Wang, M. Zhu, G. Zeng, X. Liu, C. Fang, C. Li, A three-dimensional Cu nanobelt cathode for highly efficient electrocatalytic nitrate reduction, Nanoscale. 12 (2020) 9385–9391. https://doi.org/10.1039/c9nr10743f.

[94] Y. Zhang, Y. Zhao, Z. Chen, L. Wang, L. Zhou, P. Wu, F. Wang, P. Ou, Fe/Cu Composite Electrode Prepared by Electrodeposition and Its Excellent Behavior in Nitrate Electrochemical Removal, J. Electrochem. Soc. 165 (2018) E420–E428. https://doi.org/10.1149/2.0081810jes.

[95] W. Fu, Y. Du, J. Jing, C. Fu, M. Zhou, Highly selective nitrate reduction to ammonia on CoO/Cu foam via constructing interfacial electric field to tune adsorption of reactants, Appl. Catal. B Environ. 324 (2023) 122201. https://doi.org/10.1016/j.apcatb.2022.122201.

[96] F. Yao, M. Jia, Q. Yang, F. Chen, Y. Zhong, S. Chen, L. He, Z. Pi, K. Hou, D. Wang, X. Li, Highly selective electrochemical nitrate reduction using copper phosphide self-supported copper foam electrode: Performance, mechanism, and application, Water Res. 193 (2021). https://doi.org/10.1016/j.watres.2021.116881.

[97] X. Tan, X. Wang, T. Zhou, T. Chen, Y. Liu, C. Ma, H. Guo, B. Li, Preparation of three dimensional bimetallic Cu–Ni/NiF electrodes for efficient electrochemical removal of nitrate nitrogen, Chemosphere. 295 (2022) 133929. https://doi.org/10.1016/j.chemosphere.2022.133929.

[98] S. Zhang, M. Li, J. Li, Q. Song, X. Liu, High-ammonia selective metal – organic framework – derived Co-doped Fe / Fe 2 O 3 catalysts for electrochemical nitrate reduction, 119 (2022) 2115504119. https://doi.org/https://doi.org/10.1073/pnas.2115504119.

[99] J. Wang, J. Feng, T.O. Soyol-Erdene, Z. Wei, W. Tang, Electrodeposited NiCoP on nickel foam as a self-supported cathode for highly selective electrochemical reduction of nitrate to ammonia, Sep. Purif. Technol. 320 (2023) 124155. https://doi.org/10.1016/j.seppur.2023.124155.

[100] Y. Gao, R. Wang, Y. Li, E. Han, M. Song, Z. Yang, F. Guo, Y. He, X. Yang, Regulating dynamic equilibrium of active hydrogen for super-efficient nitrate electroreduction to ammonia, Chem. Eng. J. 474 (2023) 145546. https://doi.org/10.1016/j.cej.2023.145546.

[101] W. Tao, P. Wang, B. Hu, X. Wang, G. Zhou, Accelerating the reaction kinetics from nitrate to ammonia by anion substitution in NiCo-based catalysts, J. Environ. Chem. Eng. 11 (2023) 109117. https://doi.org/10.1016/j.jece.2022.109117.

1071     [102]   Z.H. Xue, H.C. Shen, P. Chen, G.X. Pan, W.W. Zhang, W.M. Zhang, S.N. Zhang, X.H.

1072             Li, C.T. Yavuz, Boronization of Nickel Foam for Sustainable Electrochemical Reduction

1073             of Nitrate to Ammonia, ACS Energy Lett. (2023) 3843–3851.

1074             https://doi.org/10.1021/acsenergylett.3c01139.

1075     [103]   Y. Wang, S. Shu, M. Peng, L. Hu, X. Lv, Y. Shen, H. Gong, G. Jiang, Dual-site

1076             electrocatalytic nitrate reduction to ammonia on oxygen vacancy-enriched and Pd-

1077             decorated $MnO_2$nanosheets, Nanoscale. 13 (2021) 17504–17511.

1078             https://doi.org/10.1039/d1nr04962c.

1079     [104]   F. Li, Y.C. Li, Z. Wang, J. Li, D.-H. Nam, Y. Lum, M. Luo, X. Wang, A. Ozden, S.-F.

1080             Hung, B. Chen, Y. Wang, J. Wicks, Y. Xu, Y. Li, C.M. Gabardo, C.-T. Dinh, Y. Wang,

1081             T.-T. Zhuang, D. Sinton, E.H. Sargent, Cooperative CO2-to-ethanol conversion via

1082             enriched intermediates at molecule–metal catalyst interfaces, Nat. Catal. 3 (2020) 75–82.

1083             https://doi.org/10.1038/s41929-019-0383-7.

1084     [105]   E. Vichou, A. Solé-Daura, C. Mellot-Draznieks, Y. Li, M. Gomez-Mingot, M.

1085             Fontecave, C.M. Sánchez-Sánchez, Electrocatalytic Conversion of CO2 to Formate at

1086             Low Overpotential by Electrolyte Engineering in Model Molecular Catalysis,

1087             ChemSusChem. 15 (2022) 1–10. https://doi.org/10.1002/cssc.202201566.

1088